8-2005

Thermophysical Properties of the Amyloid Beta Protein from Differential Scanning Calorimetry

Donald Edward Hicks
University of Tennessee - Knoxville

To the Graduate Council:

I am submitting herewith a thesis written by Donald Edward Hicks entitled "Thermophysical Properties of the Amyloid Beta Protein from Differential Scanning Calorimetry." I have examined the final electronic copy of this thesis for form and content and recommend that it be accepted in partial fulfillment of the requirements for the degree of Master of Science, with a major in Chemical Engineering.

William V. Steele, Paul Frymier, Major Professor

We have read this thesis and recommend its acceptance:

Elizabeth Howell, Ronald Wetzel

Accepted for the Council:
Carolyn R. Hodges

Vice Provost and Dean of the Graduate School

(Original signatures are on file with official student records.)

To the Graduate Council:

We are submitting herewith a thesis written by Donald Edward Hicks entitled "Thermophysical Properties of the Amyloid Beta Protein from Differential Scanning Calorimetry." We have examined the final paper copy of this thesis for form and content and recommend that it be accepted in partial fulfillment of the requirements for the degree of Master of Science, with a major in Chemical Engineering.

William V. Steele, Co-Major Professor

Paul Frymier, Co-Major Professor

We have read this thesis and
recommend its acceptance:

Elizabeth Howell

Ronald Wetzel

Acceptance for the Council:

Vice Chancellor and Dean of Graduate Studies

THERMOPHYSICAL PROPERTIES OF THE AMYLOID BETA PROTEIN FROM DIFFERENTIAL SCANNING CALORIMETRY

A Thesis

Presented for the

Master of Science

Degree

The University of Tennessee, Knoxville

Donald Edward Hicks

August 2005

Dedication

This is dedicated to my parents; without them I would have never made it this far. To my girlfriend Sarah; thanks for staying on me to go back to graduate school. Also, to all of my friends and colleagues that supported me throughout my college career.

Acknowledgments

I would like to thank Dr. Bill Steele for providing me the opportunity to work on such a challenging project and the knowledge that he has passed on to me. I would also like to thank Dr. Paul Frymier for his support throughout my time at Tennessee and with the helpful discussions. I would also like to thank Dr. Elizabeth Howell for being on the thesis committee and providing proteins in the early stages of this project. I would also like to thank Dr. Ron Wetzel for providing the proteins, the laboratory to prepare the samples, and being on the thesis committee. I would also like to thank Angela Williams and the rest of Dr. Wetzel's lab group for instructing me on how to prepare the samples and helpful discussions. Finally, I would like to thank my family and friends for their support throughout my college experience.

Abstract

The amyloid beta (Aβ) protein is thought to play a major role in Alzheimer's Disease. Alzheimer's Disease is a late onset, progressive process associated with Aβ protein deposits and neurofibrillary tangles (Taylor 2003). Alzheimer's Disease is the most prevalent dementia (over 2/3 of all cases) in the developing world and the third leading cause of natural death in the United States (Walsh, 2001). Alzheimer's Disease is one of the amyloid diseases which are characterized by at least twenty proteins that aggregate to form insoluble fibrils with β-sheet secondary structure that affects humans and animals alike (Walsh, 2001). This research presents experimentally determined thermophysical properties such as the enthalpy of reaction, Gibbs free energy, entropy, reaction order, and activation energy using differential scanning calorimetry and predicted values from the van't Hoff equation and direct concentration measurements to better characterize the process of fibril elongation.

Table of Contents

List of Tables

List of Figures

Nomenclature

Å	angstrom
A	pre-exponential factor
Aβ	amyloid beta
A_{Ind}	area between data points in DSC curve
A_{Total}	total area under heat of reaction curve
β	beta
°C	degrees Celsius
°C/min	degrees Celsius per minute
C_A	concentration of Aβ monomer
$CaCl_2$	calcium chloride
C_{AO}	concentration of Aβ monomer at time zero
C_P	heat capacity at constant pressure
C_V	heat capacity at constant volume
DSC	Differential Scanning Calorimeter
E_a	activation energy
G	Gibbs Free Energy
g/mol	grams per mole
H	Enthalpy
HFIP	1,1,1,3,3-hexafluoro-2-propanol
HPLC	high performance liquid chromatography
K	Kelvin
k	rate constant
kcal/mol	kilocalories per mole
K_{eq}	equilibrium constant
kJ/mol	kilojoules per mole
M	molarity
mbar	millibar
mg	milligram
mL	milliliter
mL/min	milliliter per minute
mM	millimolar
mW	milliwatt
NaN_3	sodium azide
NaOH	sodium hydroxide
nm	nanometer
nM	nanomolar
PBS	phosphate buffered saline
PEG-8000	polyethylene glycol
PGE	phenyl glycidyl ether
pI	isoelectric point
R	gas constant
R*	ratio of areas

rpm	revolutions per minute
S	Entropy
s_{rl}	slope of regression line
T	temperature
t	time
TFA	trifluoroacetic acid
ThT	thioflavin T
μL	microliter
μm	micrometer
μM	micromolar
Δ	delta (change in)

Chapter 1. Introduction

The amyloid beta protein (Aβ) is one of at least twenty proteins that can form amyloid deposits, which are characterized by proteins that self-aggregate into fibrils with β-sheet secondary structure (Walsh, 2001). The first step in the aggregation reaction is the formation of nucleation sites followed by an elongation step that adds monomer to the nucleation sites to form fibrils (Lomakin, 1997).

To monitor the fibril elongation reaction, a differential scanning calorimeter (DSC) was used. The DSC detects changes in enthalpy or heat capacity of the sample and displays the electrical energy needed to maintain a nearly zero temperature difference between the sample and reference cells (Friedli, 1996). The most common study of proteins in the DSC is heat denaturation. Heat denaturation is the unfolding of a protein from the native state to a denaturated state by heating the protein. The area under the energy profile curve is the enthalpy of denaturation. For a reaction analysis, the area under the energy profile curve is the enthalpy of reaction. The object of this research was to determine whether a DSC can accurately determine the enthalpy of the fibril elongation reaction and to determine the Gibbs free energy, entropy, and activation energy of the elongation reaction.

The amount of monomer left in solution after the fibrils have stopped growing (indicating the fibrils are in thermodynamic equilibrium with the Aβ monomer) is known as the critical concentration. Once the critical concentration is determined, the equilibrium constant for the reversible reaction of monomer attaching to the fibril can be

calculated. The Gibbs free energy can be calculated from the equilibrium constant by assuming that the fibril molar concentration does not change with the addition of monomer. Once the Gibbs free energy is calculated, a van't Hoff analysis can be performed to predict the enthalpy and entropy associated with the fibril elongation reaction.

In this study, the predicted enthalpy from the van't Hoff analysis was compared to the enthalpy from the DSC. If the ratio of the enthalpy of the DSC data to the predicted enthalpy from the van't Hoff analysis is greater than one, this indicates there are intermediates in the reaction that the van't Hoff analysis did not consider (Zhuang, 1994). The intermediates could be from a side reaction taking place or from the destabilizing of the fibrils to keep the monomer bonded.

The stability of the proteins can be seen in heat capacity differences between the native protein and the protein at other temperatures. A heat capacity that is linearly increasing over a temperature range means that the proteins are highly stable (Creighton, 1992). A significant divergence from linearity means that the proteins are less stable than the native structure.

This research presents a novel approach in following a fibril elongation reaction from the direct measurement of the enthalpy change in a DSC. A van't Hoff analysis will be performed to compare the enthalpy change from the DSC to the predicted values of the enthalpy change by following the concentration profiles of the monomer. It will be shown that the data are reproducible for the critical concentrations, equilibrium constants, Gibbs free energy, enthalpy, and heat capacities.

Chapter 2. Background

2.1 Amyloid Diseases

At least twenty proteins that form fibrils with a predominant β-sheet secondary structure are known to be associated with amyloid diseases. The proteins that form these fibrils may possess any initial structure, i.e. random coil, α-helix, and others, prior to the formation of the fibrils. The Aβ monomer is one of those proteins that are known to form fibrils from an aggregation reaction. Some amyloid diseases are dementia-causing disorders that affect humans and animals alike (Walsh, 2001). Fibrils can be found in patients suffering from Parkinson's, Lou Gehrig's, Huntington's, and Prion Disease (better known as Mad Cow Disease), among others.

The most prevalent dementia (over 2/3 of all cases) in the developing world and the third leading cause of natural death in the United States is Alzheimer's Disease (Walsh, 2001). Alzheimer's Disease is a late onset, progressive process associated with Aβ protein deposits and neurofibrillary tangles (Taylor 2003). It is unclear whether the insoluble fibrils or the oligimers that are intermediates in the fibril production lead to Alzheimer's disease (Lynn, 2000).

2.1.1 Aβ Fibril Production

The Aβ monomer can naturally aggregate to form insoluble fibrils. Fibril plaques were discovered by Virchow in 1854 (Xing, 2002), but it took until 1906 until a

connection between neurofibrillary tangles and dementia in humans were found by Dr. Alois Alzheimer (http://www.alzheimers.org/generalinfo.htm). Fibrils are a group of Aβ polymers that twist with each other to form a β-sheet secondary structure (see Figure 1). The fibril formation is of interest because it is closely related to the conformational diseases, of which many are incurable, and the mechanism of fibril formation remains to be fully characterized (Žerovnik, 2002). The reaction order and rate constants have yet to be determined for the aggregation of the monomer to fibril even though the fibril elongation reaction as been reported in the literature to be pseudo first order (Naiki, 1999).

The aggregation reaction that forms the Aβ fibrils has a nucleation and an elongation step. The nucleation step of the aggregation reaction is a series of thermodynamically unfavorable elementary reactions leading to creation of a stable nucleus; nucleation is the rate determining step in the formation of fibrils (Kusumoto, 1998). The nucleation process for the Aβ protein is poorly understood. The elongation step of the aggregation reaction occurs when Aβ monomer binds reversibly to the fibril end. The elongation step is thermodynamically favorable (Hasegawa, 1999).

Due to the nucleation step, the aggregation reaction pathway exhibits a lag phase during which nucleation occurs followed by a phase of exponential fibril growth. Once the monomer and fibrils are in equilibrium with each other the exponential growth phase ends. Under typical laboratory conditions, it can take up to two weeks to reach equilibrium when starting with the pure forty unit amino acid Aβ monomer. However, equilibrium can also be reached in a matter of hours by "seeding" the monomer. The seeds are Aβ monomer that have aggregated into fibrils and then has been sonicated

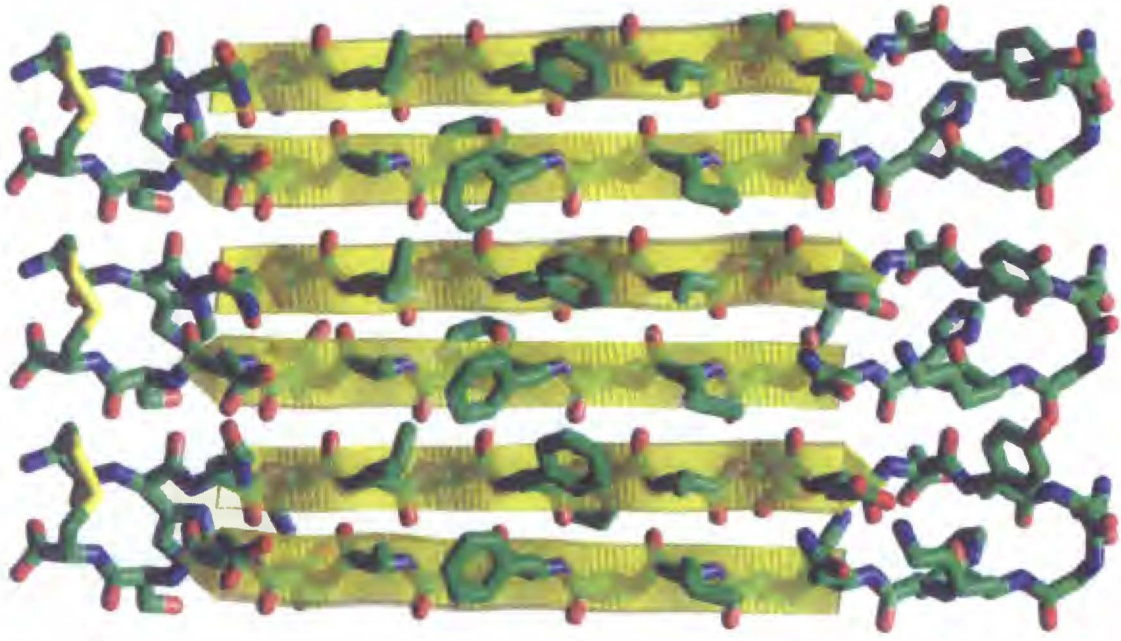

Figure 1. An energy-minimized model of fibrils formed by the 28CL peptide (β-sheets represented by yellow arrows, from Tjernberg, 2002).

to break the long fibrils down into elongation sites for controlled fibril production. Various amounts of seed can be used to vary the time required to approach equilibrium. A seed concentration of 2% by weight and with monomer concentrations around 60 μM allows the reaction to approach equilibrium in about 8 hours.

2.1.2 Aβ Protein

The Aβ protein is a naturally occurring peptide of forty to forty-two amino acids (Walsh, 1997). This study focuses on the forty unit amino acid peptide (NH_2-DAEFRHDSGYEVHHQKLVFFAEDVGSNKGAIIGLMVGGVV-CO_2H) (Kheterpal, 2000). In the human body, the Aβ protein is produced by the limited proteolysis of the β-amyloid precursor protein (APP) (Lynn, 2000). The Aβ is released from sequential proteolytic cleavages of the APP by membrane proteases referred to as β- and γ-secretases (Selkoe, 2000) The gene of the precursor protein is located on chromosome 11 (Xing, 2002). In 1984, Glenner and Wong first reported the subunit composition of amyloid filaments to residue 24. It was later shown to extend to 40 – 43 residues (Selkoe, 1991).

2.1.3 Thermophysical Properties of Aβ Protein and Fibrils

The thermophysical properties of the Aβ system are not well-known and some properties have not yet been reported in the research literature. It has been reported in literature that fibril elongation follows pseudo first-order kinetics (Naiki, 1999), which means that it is first order in fibril ends and first order in monomer concentration. The

values of previously reported physical properties are given in Table 1 (Hasegawa, 2002). The heat of reaction and entropy have not yet been reported in the literature.

2.2 Differential Scanning Calorimetry

The Perkin Elmer [Boston, MA] Pyris 1 is a power-compensation differential scanning calorimeter (DSC), which refers to the DSC having one heater and one temperature sensor per cell. Differential scanning calorimetry is a technique for measuring the energy difference necessary to establish a nearly zero temperature difference between a sample and a reference cell. It is based on the detection of changes in enthalpy or specific heat of a sample. As a reaction in the DSC proceeds, enthalpy changes cause temperature changes. The DSC constantly adjusts the temperature in the sample cell by adding or subtracting the power output to keep the sample and reference cells at a predetermined temperature. The amount of power output added or subtracted to keep the temperature constant as the reaction proceeds forward is displayed as the dependent variable (Friedli, 1996).

The power output is proportional to the specific heat of the sample. Any change in specific heat produces an exothermic or endothermic enthalpy change resulting in an extrema of power output over a period of time (Figure 2). The area between the power output curve and a line connecting any two states on the curve is proportional to the total enthalpy difference between the two states (Friedli, 1996).

Table 1. Experimentally Determined Physical Properties of Aβ Protein Aggregation Reaction (from Hasegawa, 2002).

Physical Property	**Experimental Value***
Critical Concentration	0.2 μM
Gibbs Free Energy	-11 kcal/mol
Activation Energy	10 kcal/mol
Equilibrium Constant	5×10^{7} M^{-1}

* All experiments performed at 37 °C

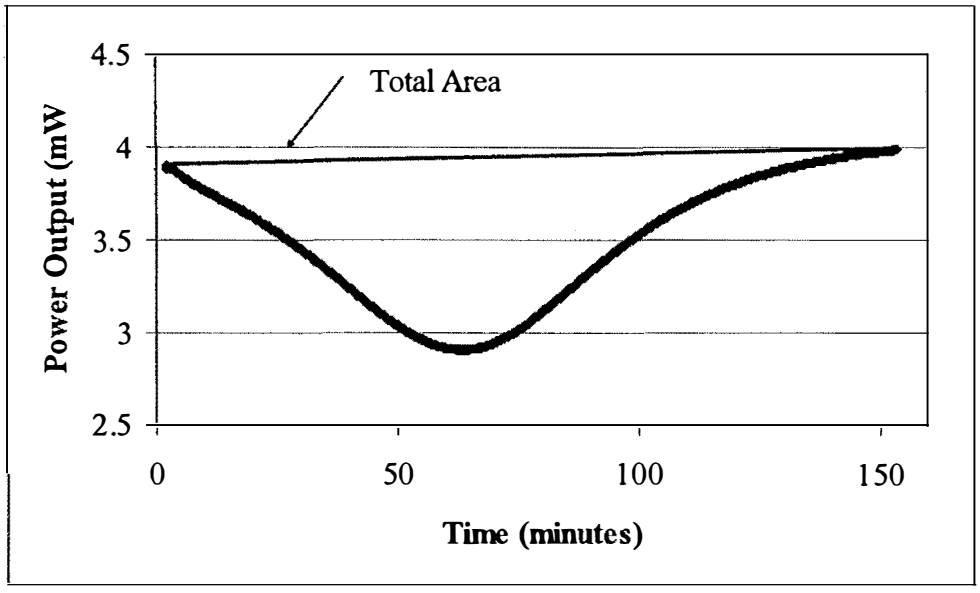

Figure 2. Isothermal scan at 98 °C of an amine-cured epoxy resin reaction used for area calculation.

2.2.1 Protein Studies using Differential Scanning Calorimetry

Thermal denaturation of proteins is the most common study performed using a DSC. Thermal denaturation is the process of unfolding proteins by using heat. The heat of denaturation can be calculated and compared to the van't Hoff enthalpy. A ratio of the heat of denaturation from the DSC to the heat of denaturation predicted by the van't Hoff analysis greater than one indicates occurrences of intermediates in the folding process (Zhuang, 1994). DSC studies can also determine whether heat denaturation is reversible by cooling the protein back to ambient temperature. If the denaturation is reversible, an exothermic peak will be present during the cooling phase. If the ratio of the enthalpy associated with the heat denaturation to the enthalpy associated with peak from cooling is one, then the protein is likely to have regained its normal structure. Reversibility of the protein denaturation is important because it relates to the amount of activity that the protein will have after cooling and determines if protein folding does reflect equilibrium and therefore the validity of treating the process using thermodynamic relationships (Dragan, 2004).

Chapter 3. Experimental Procedure

3.1 Preparation of the Aβ Monomer

Lyophilized powder form of the Aβ peptide, a forty-unit amino acid peptide, was obtained from the W. M. Keck Biotechnology Resource Center at Yale University. This was desiccated and kept in a -80 °C freezer until it was needed for preparation.

In preparing the Aβ peptide, the powder was allowed to be brought up to room temperature before opening. The balance, exterior of vial, spatula, and hands were brushed with an antistatic brush to minimize peptide loss before weighing out the powder. To determine the amount of the lyophilized peptide to weigh out, the desired concentration of the sample was multiplied by the molecular weight of the Aβ monomer (4330 g/mol) and then multiplied by the desired volume of solution. Twice the amount of peptide needed was weighed out, due to the fact that half the mass of the lyophilized peptide was water of hydration.

The following protocol was used to minimize aggregates in the final Aβ monomer solution. After the lyophilized powder had been weighed, the sample was placed in a fume hood. Trifluoroacetic acid (TFA) [obtained from Pierce, Rockford, IL] was added at 1 mL of TFA per 2 mg of weighed sample. TFA was used because it is a strong acid and can disaggregate peptides. The vial containing the solution was swirled by hand to dissolve any peptide that may have been present on the sides of the vial. The container was capped tightly and sonicated for ten minutes in a sonicator bath.

After sonicating, the sample was placed back in the fume hood. The TFA was evaporated off with a stream of argon gas. When conducted properly, the evaporation step will result in a thin "film" of the peptide around the bottom of the vial containing the sample. One milliliter of 1,1,1,3,3-hexafluoro-2-propanol (HFIP) [obtained from Acros through Fisher Scientific, Fair Lawn, NJ] per 2 mg of weighed powder was then added. HFIP is used to help evaporate off trace amounts of TFA and to help disaggregate the peptide. The sample was incubated for one hour at 37 °C, to give time for the film at the bottom of the sample vial to dissolve and to ensure complete disaggregation.

The sample was placed back in the fume hood. The HFIP was evaporated off using an argon gas sweep as before. More HFIP was added at 1 mL per 2 mg of lyophilized powder to ensure that as much peptide as possible was in solution and that there was no TFA present in the sample. At this point, the sample was frozen at -20 °C for multiple uses in the coming months as a stock solution.

When an experiment was to be conducted, the frozen sample was allowed to thaw at room temperature. Aliquots of 125 μL were taken from the sample and placed into test tubes. The HFIP was evaporated off with an argon gas sweep as described before. After removal of HFIP, the sample was lyophilized a minimum of one hour at operational condition of approximately 10^{-3} mbar with a cold trap operated at -46 °C to ensure complete dehydration.

Sodium hydroxide (NaOH) at a concentration of 2 mM (pH 9.5) is needed to dissolve the protein back into solution while maintaining a basic pH if traces of TFA are present. A slightly acidic pH will to isoelectric precipitation of the Aβ monomer whose pI is about 5.5. Since the amount of NaOH to add to each sample was half of the total

volume, it was calculated by dividing the desired final sample volume in half and then dividing by the number of test tubes that were used. Once the NaOH was added, the solution was allowed to stand for at least five minutes to allow the monomer to go into solution. The vials were gently tilted and twisted by hand to make sure that the NaOH would be in contact with all of the film.

The amount of 2X phosphate buffered saline (PBS) with 0.1% sodium azide (NaN_3) added to each of the vials was the same volume as the NaOH. The NaN_3 was not placed in the buffer for the heat of reaction and heat capacity measurements. The powder form of PBS was ordered from Fisher Scientific [Catalog No. BP399-1] with a10X strength in 1 L of water and then diluted to 2X strength. The PBS contained 8% sodium chloride, 1.4% sodium phosphate dibasic, <1% potassium chloride, <1% potassium phosphate monobasic, and the rest was filtered, deionized water (0.137 M sodium chloride, 0.0027 M potassium chloride, 0.0119 M phosphate buffer in final 1X solution in buffer). The amount of sodium azide required to eliminate unwanted bacterial growth was 0.05% of the buffer (mass-to-volume).

The resulting mixtures were then spun on a bench top centrifuge at 20,000 rpm (20,800 x g) for 60 minutes at 4 ºC to remove any unwanted aggregates from the monomer. The supernatant was transferred to smaller vials for experimentation (~ 80% of total volume). The monomer concentration of the supernatant was determined by using an Agilent 1100 series high performance liquid chromatography (HPLC), with an Agilent Technologies [Palo Alto, CA] 80Å Zorbax StableBond column (3.0 mm x 150 mm, 5 μm particle size) with optima water (Fisher Scientific) and 0.05% TFA as Buffer

A and acetonitrile (Fisher Scientific) and 0.05% TFA as Buffer B. The gradient used was 1 – 51% B in twenty-five minutes.

3.2 DSC Calibration

A Perkin Elmer Pyris 1 Differential Scanning Calorimeter (DSC) was calibrated with the melting points of indium and lead, 156.65 °C (Strouse, 2001) and 327.5 °C (Briggs, 1943), respectively. All experiments were run with a 20 mL/min of nitrogen (obtained from Airgas) purge gas, an initial power output of 20 mW, and a standard sampling rate of one sample per second. The indium was obtained from Aldrich [St. Louis, MO] with 99.999+% purity. A sample was weighed out on a microbalance. The indium was then placed in aluminum "pans" from TA Instruments [New Castle, DE; Part No.'s 900796.901 (bottom) and 900790.901 (top)] in the sample cell and an empty aluminum pan was placed in the reference cell. The initial temperature was set at 150 °C with a scan rate of 5 °C/min up to 165 °C. The temperature and enthalpy change were recorded and placed in the calibration file. For the lead (obtained from Aldrich, 99.9995% purity) calibration, the same process was followed except that the initial temperature was set for 310 °C with a scan rate of 5 °C/min until the final temperature of 335 °C.

The melting of indium and lead take place over a couple of seconds. The DSC also needed to be calibrated on a time scale. Two reactions were selected for this additional calibration. The first reaction was the trypsin-catalyzed hydrolysis of benzoylarginine ethyl ester (BAEE). This reaction takes place over 35 minutes and has a

heat of reaction equal to -11.45 kcal/mol at 25 °C (Todd, 2001). A solution of 9.6 nM trypsin in 200 mM Tris-HCl, at a pH of 8.0, 50 mM calcium chloride ($CaCl_2$), and 0.2% by weight PEG-8000 was prepared. This solution was made in three steps. The first solution (Solution A) made was a 1750 μL solution containing 1000 μL of 1 M Tris-HCL [Fisher Scientific] with 750 μL of deionized water. Ten milligrams of trypsin (Laboratory Grade from Fisher Scientific) were added to 500 mL of deionized water. Solution B contained 1 mL of the trypsin solution that was diluted in 9 mL of deionized water. For Solution C, 11.7 mg of BAEE [Fisher Scientific] were added to 100 mL of deionized water. Five hundred microliters of Solution A were added to Solution B in a tube along with 2 mg of PEG-8000 [Fisher Scientific] and 7 mg of $CaCl_2$ [Fisher Scientific]. Ten microliters of this solution were placed in two aluminum "pans", holding approximately 25 μL each, along with 10 μL of deionized water added to one of the pans and placed in the reference cell. Ten microliters of the BAEE solution (Solution C) were added to the other aluminum pan. A matching cap was crimped onto the pan and the pan was placed in the sample cell.

Amine-curing of phenyl glycidyl ether (PGE) with aniline was used as an additional calibration reaction. This reaction takes place over 400 minutes with a heat of reaction of -24 ± 1 kcal/mol at 98 °C (Sweir 2003). The PGE [Fisher Scientific] and aniline [Acros, through Fisher Scientific] were combined in stoichiometric proportions (one-to-one, on a molar basis). An aluminum pan was weighed and 6.7 μL of aniline was added then weighed again. Ten microliters of the PGE was added to the aluminum pan. The pan was capped as described previously and placed in the sample side of the DSC, whereas an empty capped pan was placed in the reference side. After the amine-curing of

PGE, the aluminum pan was weighed again. The weight of the pan with aniline was subtracted from the weight of the pan with the amine-cured PGE. The weight of the aniline and PGE was multiplied by their respective molecular weights, 93.13 g/mol and 150.18 g/mol. The reactant present in the lower molar amount was the limiting reactant. The area produced by the DSC curve was then divided by the moles of the limiting reactant yielding the heat of reaction.

3.3 Heat of Reaction Measurements

For the heat of reaction measurements, the Aβ monomer was kept in ice along with its buffer and fibril seeds in separate vials. The fibril seeds are Aβ monomer allowed to aggregate to form a polymer with a β-sheet secondary structure and sonicated to break up the fibrils into shorter pieces with more growing ends as discussed previously (Williams, 2004). The seeds increase the reaction rate decreasing the time required for an experiment. This decreases the data points needed for an experiment thus not "locking up" the computer.

The DSC program used for determining the heat of reaction was an isothermal scan at 37 °C for 1,320 minutes. Initial conditions for this program remain the same as for the calibration reactions; the nitrogen purge stream was set at 20 mL/min with a standard sampling rate of one sample per second.

An empty gold-coated high-pressure pan [Perkin Elmer, Part No. N5200001] was placed in the reference cell. Thirty microliters of the monomer were put into a gold-coated high-pressure pan followed by adding 3 μL of seed. The gold-coated high-

pressure pan was placed in the chuck and the lid was screwed into place. The gold-coated high-pressure pan was placed in the sample cell. The program was started to allow the sample and reference cells to equilibrate to 37 °C. The area under the curve was calculated by integrating from the start point of the reaction to the point at where the power supplied came back to the starting power (refer to Figure 2). The area was then divided by the weights of monomer and seed that were added to the pan, which were determined by HPLC, and multiplied by the molecular weight of the monomer yielding the heat of reaction in Joules per mole of Aβ monomer.

3.4 Heat Capacity Measurements

Heat capacity measurements were performed on the Aβ monomer and the associated Aβ fibrils. An empty gold-coated high-pressure pan was sealed and weighed in a microbalance. A piece of sapphire, obtained from NIST [Boulder, CO; standard sample SRM720], was placed in a gold-coated high-pressure pan, not sealed, to be weighed. Also, the individually sealed pans holding the monomer, fibril, and the buffer were weighed. The weight of the empty pan was subtracted from all the other samples. The weights of the samples, after pan subtraction, were used to calculate the specific heats of reaction.

The program used for the heat capacity measurements was set with an initial temperature of 27 °C and initial power of 20.000 mW. The nitrogen purge stream was set at 20 mL/min. A standard sampling rate of one data point per second was used. The method also consisted of holding at temperature for one minute followed by a 2.5 °C/min

scan rate for two minutes (a total change of 5 °C) and then repeating until the final temperature of 82 °C was reached. The program held for one minute at the final temperature and then cooled to the loading temperature of 26 °C.

The empty pan was placed in the reference cell. One sample at a time was placed in the sample cell. One of the samples was an empty gold-coated high-pressure pan that was empty. An empty pan is used to determine the specific heat associated with the difference in weights of the gold-coated high-pressure pans.

After the last sample, all data files containing the power output and temperature of the cells were converted to text files for numerical integration. The power data were integrated using Simpson's 1/3 Rule (Kreyszig, 1999) which yields the area under each of the peaks (Figure 3) for all of the samples. Since the sapphire heat capacity is known, the heat capacity of the pan and the sample can be calculated from the ratio of their peak areas to the peak areas of the sapphire. The contribution to the heat capacity from the pan was subtracted from the sample resulting in the heat capacity of the sample itself.

3.5 Critical Concentration of the Aβ Monomer

The amount of Aβ monomer that remains in the solution after the fibril elongation reaction reaches equilibration is known as the critical concentration. The critical concentrations were found at 19 °C, 28 °C, 37 °C, 46 °C, 55 °C, and 64 °C. The Aβ monomer was prepared as described previously, but the solution was centrifuged at 100,000 rpm (315,000 x g) overnight at 4 °C instead of 60 minutes at 20,000 rpm (20,800 x g) at 4 °C. The increased speed was used for more of the small oligimers to spin out of

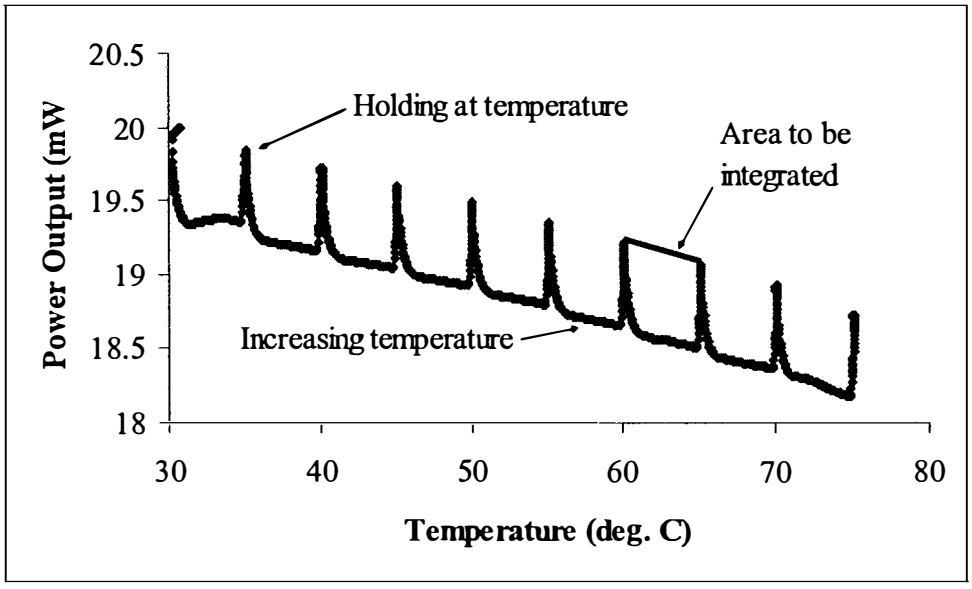

Figure 3. Heat capacity data.

solution and form a small pellet. Fibril seed was added at 2% by weight to the solution. Then 230 μL of the monomer solution was aliquotted into six vials and placed into a water bath at each temperature. The rest of the stock solution was transferred to a smaller vial, Vial A, and placed in the 37 °C bath.

A spectrophotometric assay based on thioflavin T was performed each day for Vial A until fibril formation was judged to have come sufficiently to equilibrium. This was determined by monitoring the rise in ThT fluorescence (Figure 4). The dye-binding properties of ThT are a result of the β-sheet content within the Aβ fibrils (Fezoui 2002). The excitation wavelength is 450 nm with an emission wavelength of 482 nm. ThT was obtained from Acros [Catalog No. AC21176-0250] then dissolved in 1X PBS and 0.05% NaN_3 to make a 1.5 mM solution of ThT. For use in the Perkin Elmer Luminescence Spectrometer LS50B, the ThT was diluted to 15 μM concentration. The sample included 1.25 μg of Aβ protein and 400 μL of ThT solution.

After ThT fluorescence for Vial A was judged to have sufficiently reached a plateau, 170 μL of the seeded elongation reaction at 37 °C were aliquotted into six separate vials to be placed in each temperature bath. This was done as verification on the critical concentration at each temperature. Forty microliters of each of the twelve samples were placed in a bench top ultracentrifuge for 30 minutes at 4 °C and 100,000 rpm (315,000 x g). Ten microliters of the supernatant of each of the twelve samples were added to 110 μL of a 0.1% TFA solution for testing in the HPLC. The monomer concentration was monitored by HPLC until the area under the peak of the monomer that was placed in the water baths just after seeding equaled the area under the peak for the

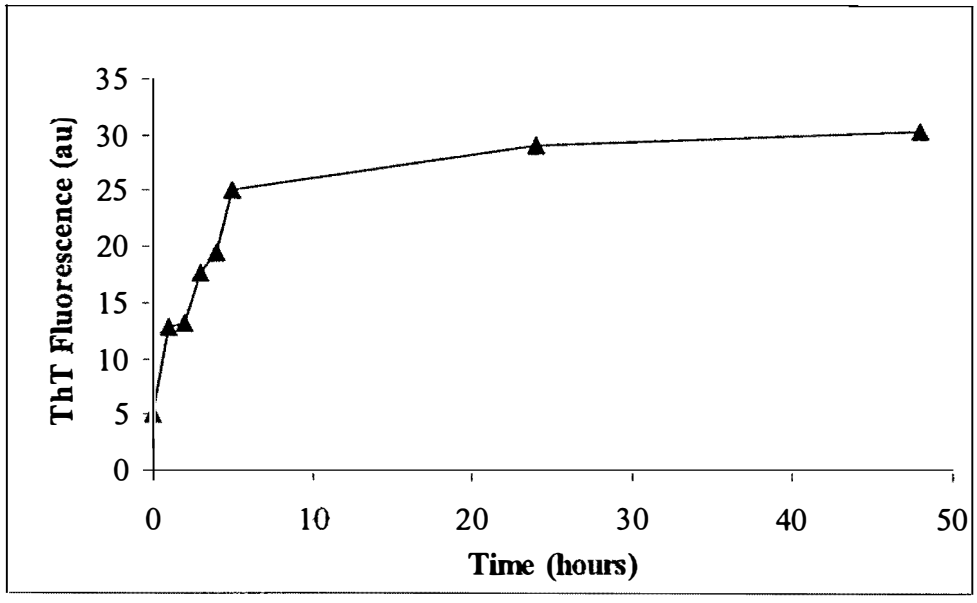

Figure 4. Thioflavin fluorescence for a 2% seeded monomer aggregation with a starting monomer concentration of 82.7 μM.

monomer that was reacted at 37 °C and then placed in the water baths. The concentration measurements were done daily. The critical concentration was determined by the area under the peak at 17.5 minutes into the HPLC run (Figure 5) with a standard curve for the weight of Aβ monomer that had previously been determined in the lab.

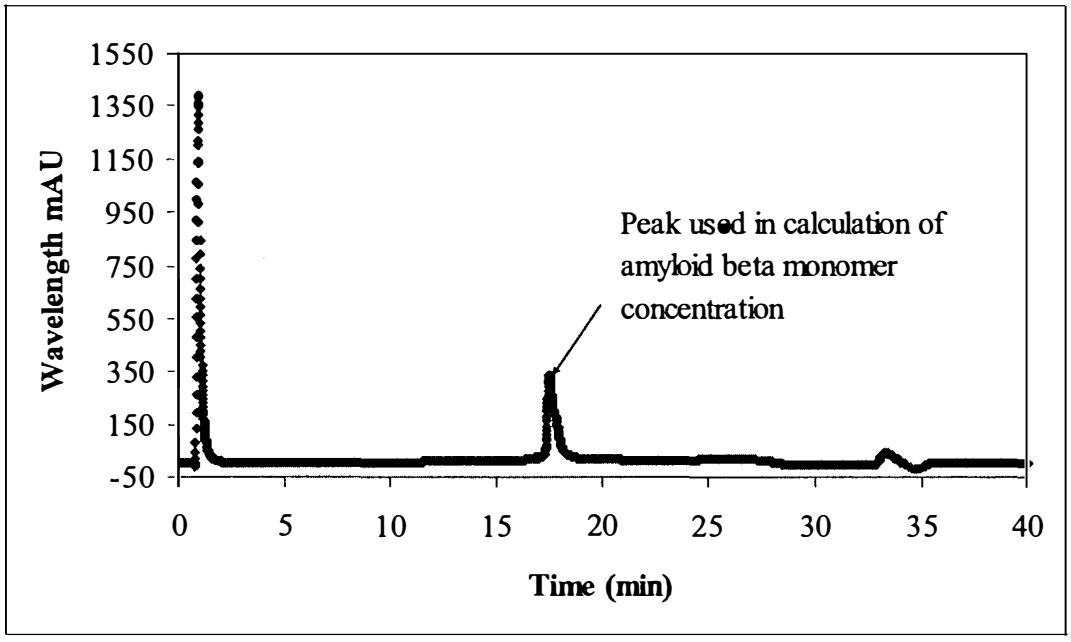

Figure 5. HPLC chromatograph of a sample of Aβ monomer.

Chapter 4. Results

4.1 Heat of Reaction

The first step in determining the heat (enthalpy) of reaction (ΔH) for fibril elongation is to determine the energy profile of the buffer. The energy profile of the buffer is the amount of electrical power required to maintain the buffer at the desired temperature as compared to the reference cell which contained no solution (only air). The energy profile that maintains water, which is inert, at a constant temperature is seen in Figure 6. Because the water does not exhibit an enthalpy change, the energy profile is horizontal. When the DSC detects an enthalpy change, there is a spike in the energy profile. The energy profile that maintains the buffer solution at each of three temperatures (28 °C, 37 °C, and 46 °C) can be seen in Figures 7, 8, and 9. For systems in which a reaction occurs (such as fibril formation), the energy measured by the DSC begins to increase (endothermic) or decrease (exothermic) as the reaction proceeds. As the reaction approaches its endpoint, the energy profile becomes horizontal (refer to Figure 2). If multiple reaction steps occur in series, a succession of increases or decreases in the energy input will be seen, separated by periods when the energy profile is relatively horizontal. As seen in Figures 7, 8, and 9, there appears to be multiple reactions occurring in the buffer and in Figures 10, 11, and 12 there appears to be multiple reactions occurring in the Aβ-buffer mixture. The early portion of the profile indicates an endothermic reaction was occurring whereas the later portion of the profile indicates an exothermic reaction was occurring. In the analysis that follows, sometimes

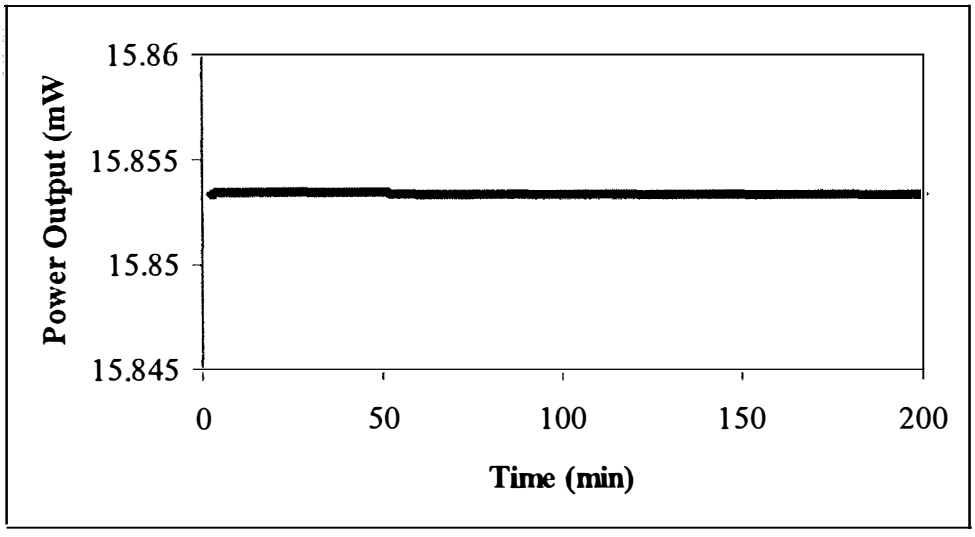

Figure 6. Energy profile of water.

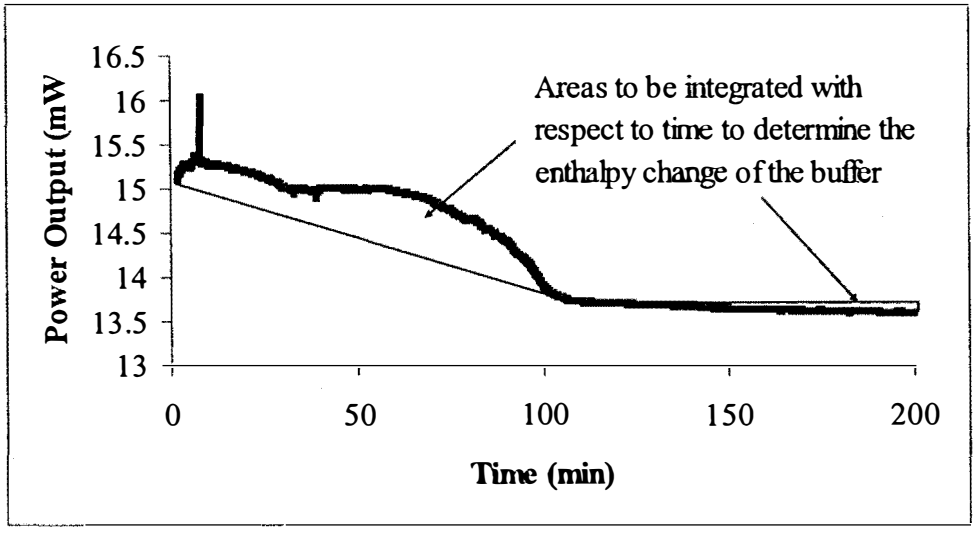

Figure 7. Energy profile of the NaOH – 2X PBS buffer at 28 °C truncated at 200 minutes.

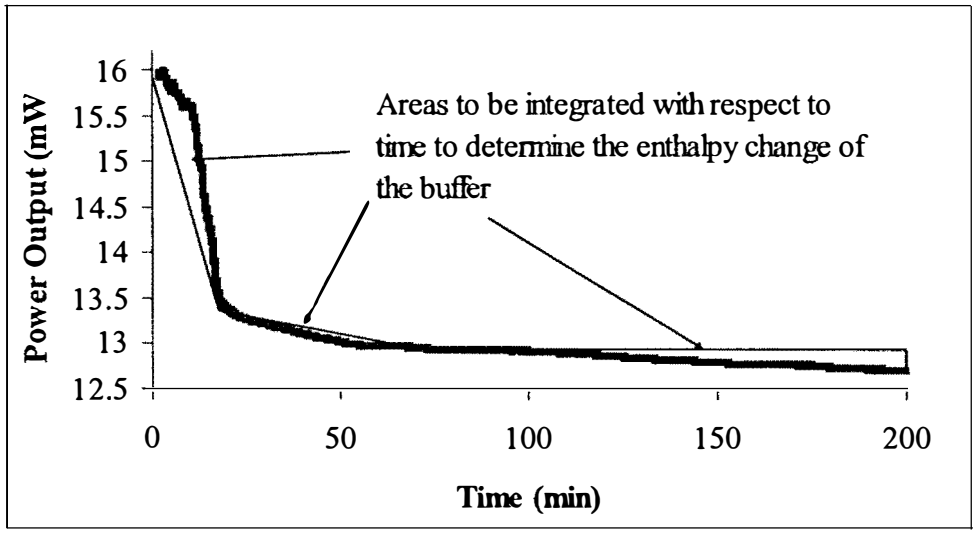

Figure 8. Energy profile of the NaOH – 2X PBS buffer at 37 °C truncated at 200 minutes.

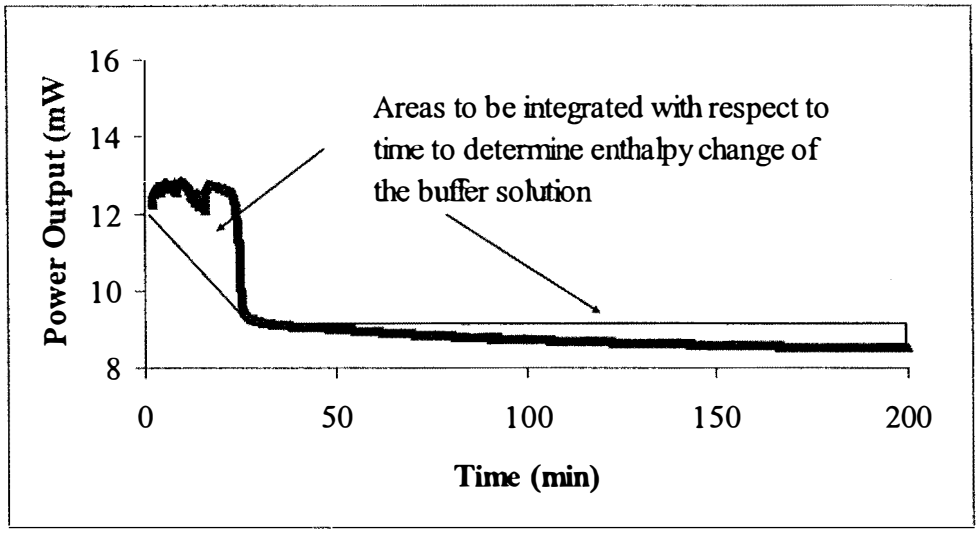

Figure 9. Energy profile of the NaOH – 2X PBS buffer at 46 °C truncated at 200 minutes.

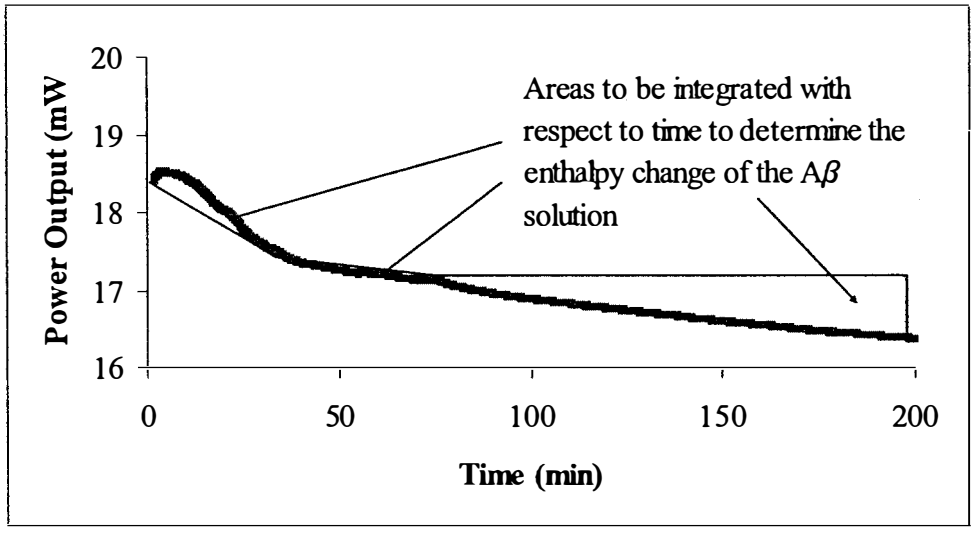

Figure 10. Energy profile of the Aβ solution at 28 °C truncated at 200 minutes.

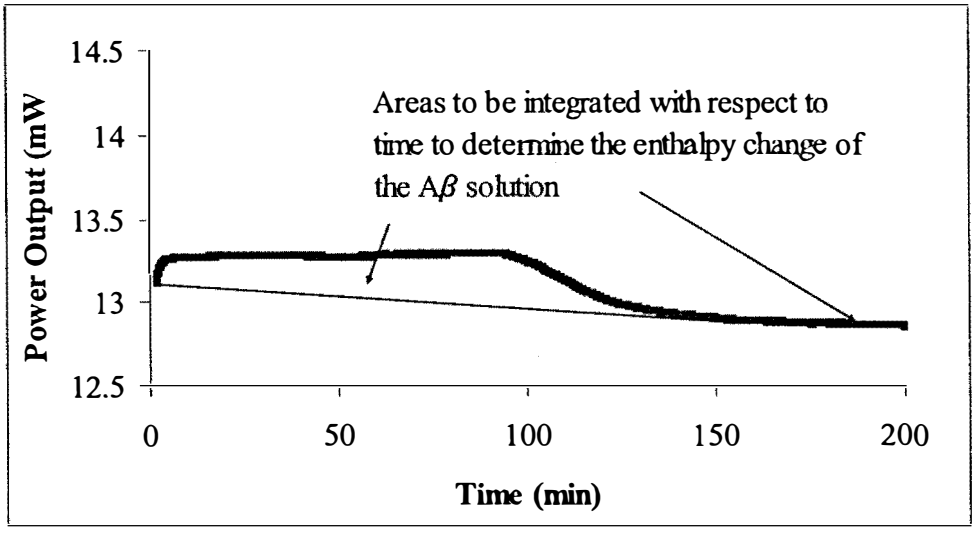

Figure 11. Energy profile of the Aβ solution at 37 °C truncated at 200 minutes.

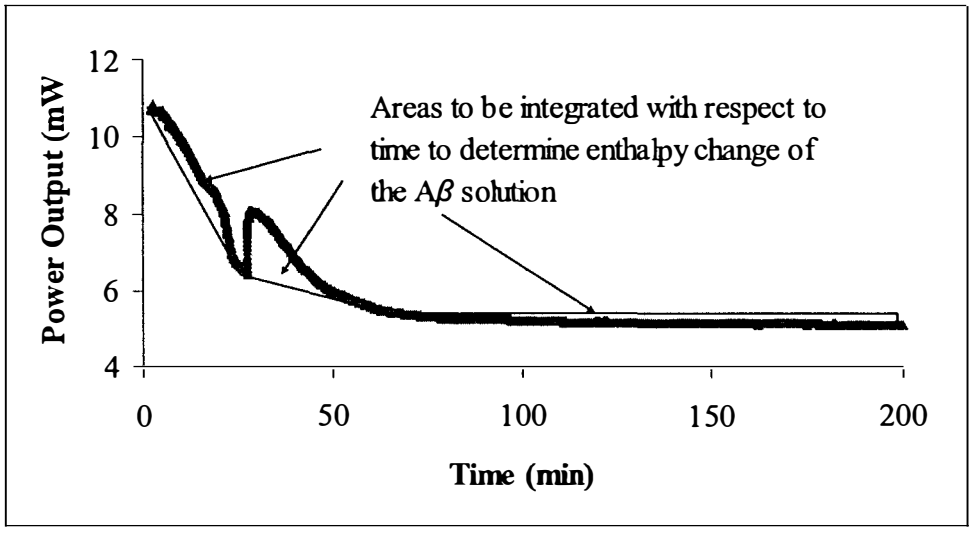

Figure 12. Energy profile of the Aβ solution at 46 °C truncated at 200 minutes (it is not known why the second extrema is occurring).

the entire energy profile was integrated to determine the enthalpy of the entire process; this enthalpy change is called the total enthalpy change. Other times, only the portion of the energy profile associated with the first reaction (believed to be the actual fibril elongation reaction) was integrated; this is called the enthalpy change for the fibril elongation portion of the reaction alone. The energy profiles of the buffer indicate that the buffer produces significant enthalpy changes even when held at constant temperature. The enthalpy change is probably due to the NaOH reacting with air and the phosphate ions in the PBS going to an equilibrium mixture at the desired temperature. Because the fibril elongation reaction takes place in this buffer, the contribution of the buffer to the total enthalpy change must be subtracted to measure the enthalpy change associated with fibril extension alone. Temperatures of 28 °C, 37 °C, and 46 °C were used to determine the enthalpy change of the buffer alone and the heat of reaction for fibril elongation in buffer.

The following protocol is used to determine the enthalpy change associated with the fibril elongation reaction itself, without the contribution from the buffer. The relationship between the enthalpy change associated with just the protein (ΔH_P [cal]), the enthalpy change of the buffer (ΔH_B [cal], Table 2), and the enthalpy change of the Aβ-buffer mixture (ΔH_M [cal], Table 3) can be seen in Equation 1. Writing the extensive

$$\Delta H_P = \Delta H_M - \Delta H_B \tag{1}$$

enthalpy changes as the product their specific (per unit mass) counterparts (denoted as $\hat{H}$' for the specific enthalpy per mass of substance in cal/gram) and their respective masses, we have Equation 2, where m_P, m_B, and m_M are the masses of the protein in the mixture,

Table 2. Total enthalpy changes associated with the buffer.

T (°C)	m_B (mg)	Total Enthalpy Change		Fibril Elongation Portion Alone	
		ΔH_B (cal)	$\Delta \hat{H}_B'$ (cal/g_B)	ΔH_B (cal)	$\Delta \hat{H}_B'$ (cal/g_B)
28	33	-8	-230	-0.07	-2
37	33	-7	-208	-0.5	-14
46	33	-8	-230	-0.2	-6

B ≡Buffer

Table 3. Total enthalpy changes associated with the Aβ-buffer mixture.

T (°C)	m_M (mg)	Total Enthalpy Change		Fibril Elongation Portion Alone	
		ΔH_M (cal)	$\Delta \hat{H}_M'$ (cal/g_M)	ΔH_M (cal)	$\Delta \hat{H}_M'$ (cal/g_M)
28	33	-1.3	-39	0.2	5
37	33	-0.2	-6	0.1	3
46	33	-0.1	-3	0.3	8

M ≡Mixture

$$m_P \Delta \hat{H}'_P = m_M \Delta \hat{H}'_M - m_B \Delta \hat{H}'_B \quad (2)$$

the buffer, and the mixture in grams. The mass of the buffer was 33 mg while the mass of the protein in the buffer was 0.02 mg, so the mass of the mixture of the two, m_M, is essentially equal to m_B, so m_M can replace m_B in Equation 2. Both sides are divided by the mass of the protein in the solution (Equation 3) to solve for the enthalpy change

$$\Delta \hat{H}'_P = \frac{m_M}{m_P}\left(\Delta \hat{H}'_M - \Delta \hat{H}'_B\right) \quad (3)$$

associated with the fibril elongation reaction alone ($\Delta \hat{H}_P$ [cal/g_P]). $\Delta \hat{H}_P$' is multiplied by the molecular weight of the Aβ protein (4330 g/mol) to yield the enthalpy change on a per mol Aβ monomer basis ($\Delta \hat{H}_P$ [cal/mol_P]).

Figures 10, 11, and 12 show the energy profiles of the Aβ-buffer mixture. Ideally, the enthalpy change associated with the buffer would be small when compared to that of the Aβ-buffer mixture. In this case, the "background" enthalpy change (that of the buffer) would not obscure the enthalpy change associated with fibril elongation. However, in the experiments performed in this study, the "background" enthalpy change is of the same order as (and is in one case larger than) that of the Aβ-buffer mixture (compare $\Delta \hat{H}_M$' and $\Delta \hat{H}_B$' in Tables 2 and 3). Therefore, large errors can result when two large numbers are subtracted to yield a relatively small number. This must be borne in mind when the data are analyzed.

Since the heat capacity of water hardly changes with temperature and most of the buffer is water, the integration of the energy profile per gram of buffer is expected to be the same at each temperature for every experiment. The result of the subtraction of the integration of the energy profiles is the enthalpy change associated with the fibril

elongation reaction alone. The average total enthalpy at each temperature along with their respective 95% confidence intervals for the fibril elongation reaction is seen in Table 4. In the DSC data for fibril elongation, there are two different reactions occurring (Figures 10, 11, and 12). The first reaction is endothermic (Table 5) whereas the second reaction is exothermic. The first reaction is believed to be the fibril elongation since the nucleation step of the reaction has been eliminated due to seeding of the reaction; the elongation step of the reaction proceeds immediately. The elongation step comes to completion in less than eight hours when an initial monomer concentration of 60 μM is used along with a seed percentage of two percent by weight. The second reaction could be a higher order reaction where conformational changes are occurring but further investigation of the later reaction was not pursued.

4.1.1 Reaction Order, Rate, and Activation Energy

An attempt was made in this analysis to independently determine the reaction order using the energy profile of the fibril elongation reaction. For a first order reaction, Equation 4 (Benson, 1960) is used. $C_A(t)$ is the concentration of Aβ monomer at time t

$$\ln\left(\frac{C_A(t)}{C_{AO}}\right) = -kt \tag{4}$$

during the reaction and C_{AO} is the Aβ monomer concentration at time zero (the initial concentration). The value of the ratio $\frac{C_A(t)}{C_{AO}}$ in Equation 4 is given by Equation 5,

Table 4. Total enthalpy changes of the buffer, mixture of monomer and buffer, and the fibril elongation reaction.

T (°C)	$\Delta\hat{H}_B'$ (cal/g_B)	$\Delta\hat{H}_M'$ (cal/g_M)	m_M (mg)	m_P (μg)	$\Delta\hat{H}_P'$ (cal/g_P)	$\Delta\hat{H}_P \times 10^{-3}$ (kcal/mol_P)
28	-230	-39	33	21	300,000	1,300 ± 250
37	-208	-6	33	22	303,000	1,300 ± 87
46	-230	-3	33	22	340,000	1,500 ± 22

B ≡Buffer M ≡Mixture P ≡Protein

Table 5. Enthalpy changes for the fibril elongation portion of the reaction alone for the buffer, mixture of monomer and buffer, and the fibril elongation reaction.

T (°C)	$\Delta\hat{H}_B'$ (cal/g_B)	$\Delta\hat{H}_M'$ (cal/g_M)	m_M (mg)	m_P (μg)	$\Delta\hat{H}_P'$ (cal/g_P)	$\Delta\hat{H}_P \times 10^{-3}$ (kcal/mol_P)
28	-2	5	33	21	11,000	48 ± 27
37	-14	3	33	22	25,500	110 ± 40
46	-6	8	33	22	21,000	91 ± 55

B ≡Buffer M ≡Mixture P ≡Protein

$$\frac{C_A(t)}{C_{AO}} = \frac{\int_0^t Pdt}{\int_0^{t_f} Pdt} \tag{5}$$

where P is the power output and t_f is the final time (the time at the end of the experiment). The integrals in Equation 5 are evaluated numerically using Simpson's 1/3 rule, as discussed earlier. The DSC is set at a standard sampling rate of one data point every one second, so one second was used as the time interval in the integration by Simpson's 1/3 rule.

The reaction order and rate constant, k, are found by plotting the ratio $\frac{C_A(t)}{C_{AO}}$ indicated in Equation 5. Defining the ratio $\frac{C_A(t)}{C_{AO}}$ as R* for brevity, a plot of $\ln(R^*)$ as a function of t will yield a straight line with a slope of (–k) if the reaction is first order, as indicated in Equation 6 (Figure 13).

$$\ln(R^*) = -kt \tag{6}$$

Since the regression line in Figure 13 is not linear by this analysis, the same general process is repeated for a second order reaction (Equation 7 (Benson, 1960), Figure 14). Equation 7 is rewritten in much the same way as Equation 4 to use the

$$\frac{C_{AO}}{kC_A} - \frac{1}{k} = C_{AO}t \tag{7}$$

DSC data (Equation 8), where $A_{Total} = \int_t^{t_f} Pdt$. The plot of $A_{Total}t$ versus $\frac{1}{R^*}$ will yield a

$$\frac{1}{kR^*} - \frac{1}{k} = A_{Total}t \tag{8}$$

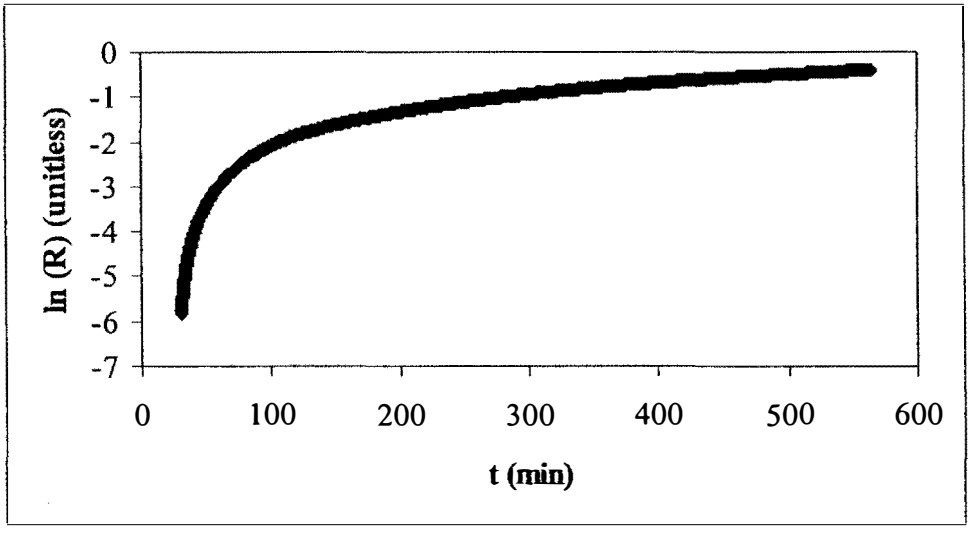

Figure 13. First order reaction plot from DSC experiment.

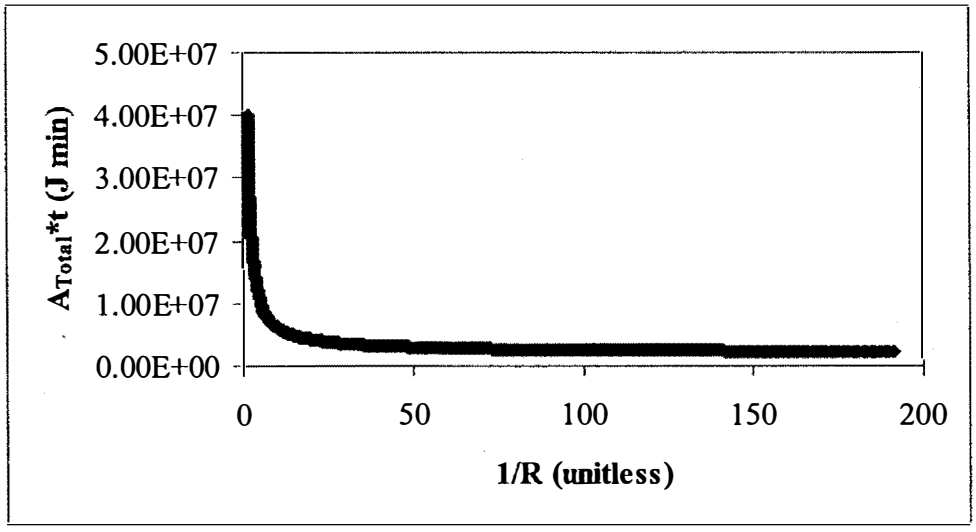

Figure 14. Second order reaction plot from DSC experiment.

straight line if the reaction is second order. The rate constant for a second order reaction plot is the inverse of the slope and the inverse of the y-intercept.

As seen in Figures 13 and 14, the fibril elongation reaction is not shown to be a first or second order reaction by this analysis. The general form of the second order reaction equation was then used (Equation 9) to determine the order of the reaction;

$$\frac{1}{(n-1)kR^{*(n-1)}} - \frac{1}{(n-1)k} = A_{Total}^{(n-1)} * t \tag{9}$$

where n is the reaction order and the rest of the variables are as described earlier. The fibril elongation reaction is shown in this analysis to be a third order reaction for temperatures of 28 °C, 37 °C, and 46 °C in Figures 15, 16, and 17.

The rate constants at each temperature are determined using the slope of the regression line. The slope is chosen because it is a more accurate description of the data than the y-intercept due to the y-intercept being an extrapolation. To solve for the rate constants from the slope, Equation 10 is used where s_{rl} is the slope of the regression line.

$$k = \frac{1}{2s_{rl}} \tag{10}$$

Using the rate constants (Table 6) determined from Equation 10 and then rearranging Equation 11 (Alberty, 1997) for the rate constant to yield a straight line

$$k = Ae^{\frac{-E_a}{RT}} \tag{11}$$

(Equation 12) (Benson, 1960). The activation energy (E_a) and pre-exponential

$$\ln k = \ln A - \frac{E_a}{RT} \tag{12}$$

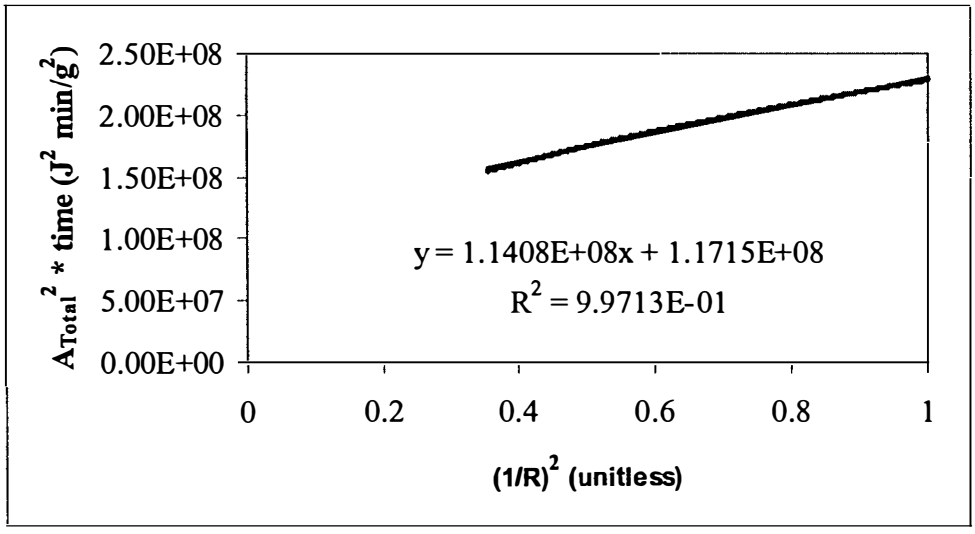

Figure 15. Third order reaction plot for 28 °C with regression line.

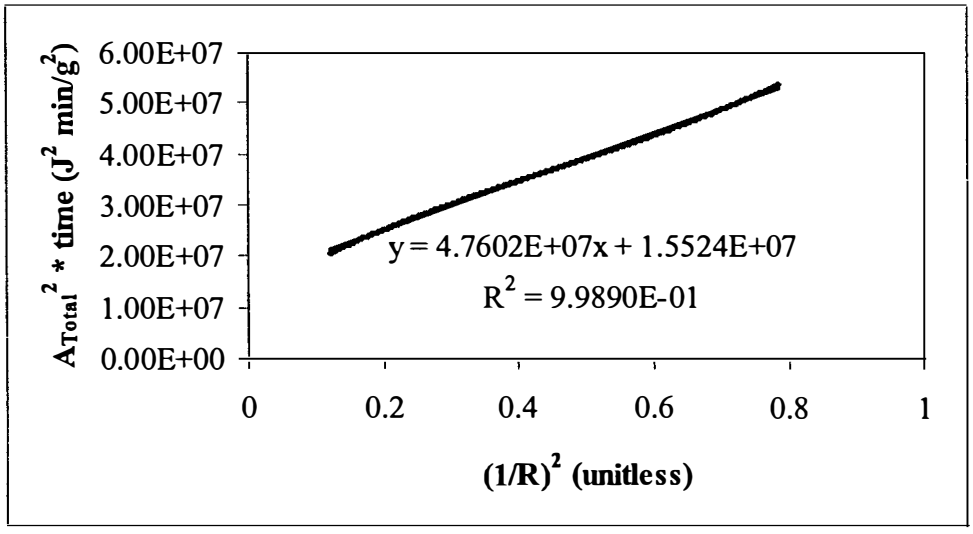

Figure 16. Third order reaction plot for 37 ºC with regression line.

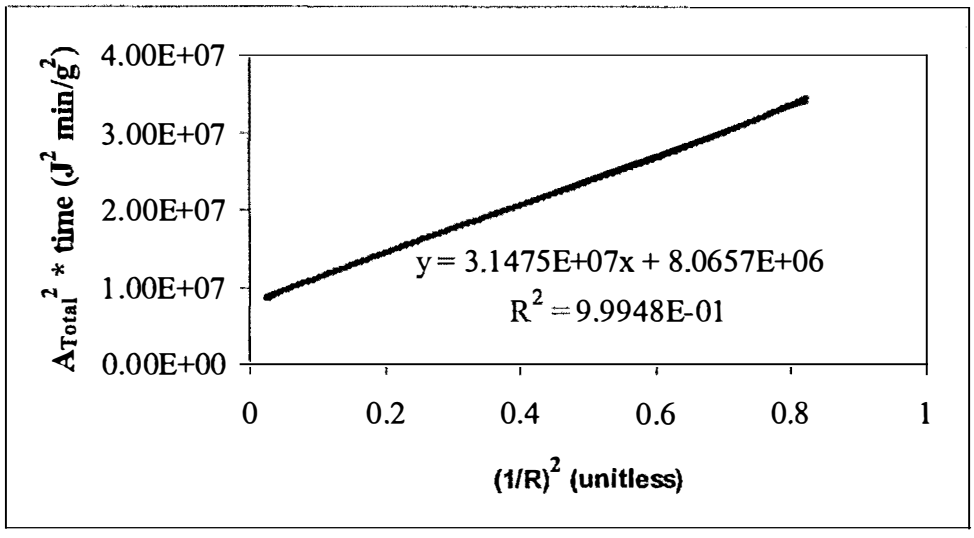

Figure 17. Third order reaction plot for 46 °C with regression line.

Table 6. Rate constant values as a function of temperature.

Temperature (°C)	**k x 10^8 ($M^{-2}min^{-1}$)**
28	0.4
37	1.1
46	1.6

rate factor (A) are determined by plotting $\ln k$ versus $\frac{1}{RT}$ (Figure 18).

The regression line from Figure 18 is $y = -13.7x + 3.7$. The slope of regression line is the negative of the activation energy and the y-intercept is the natural log of the pre-exponential rate factor (A). The activation energy determined from the regression line is 13.7 kcal/mol. The pre-exponential rate factor calculated from the regression line is 40.4 $M^{-2}min^{-1}$.

4.2 Heat Capacity

The DSC can also be used to calculate the heat capacity at constant volume (C_V). Figures 19 and 20 show the experimentally determined values of C_V for the Aβ monomer and associated fibrils. The values for the fibrils are given as per gram of fibril; there is not a molecular weight associated with the fibrils because monomer molecules are attaching and detaching to the fibrils yielding a different weight at each step. For comparison purposes, the heat capacity of the monomer is also given as per gram of monomer basis.

4.3 Critical Concentration

The concentration of Aβ monomer left in solution after equilibrium is reached with the fibrils is known as the critical concentration (Williams, 2004). The Aβ monomer concentration was followed by HPLC while the fibril formation was followed

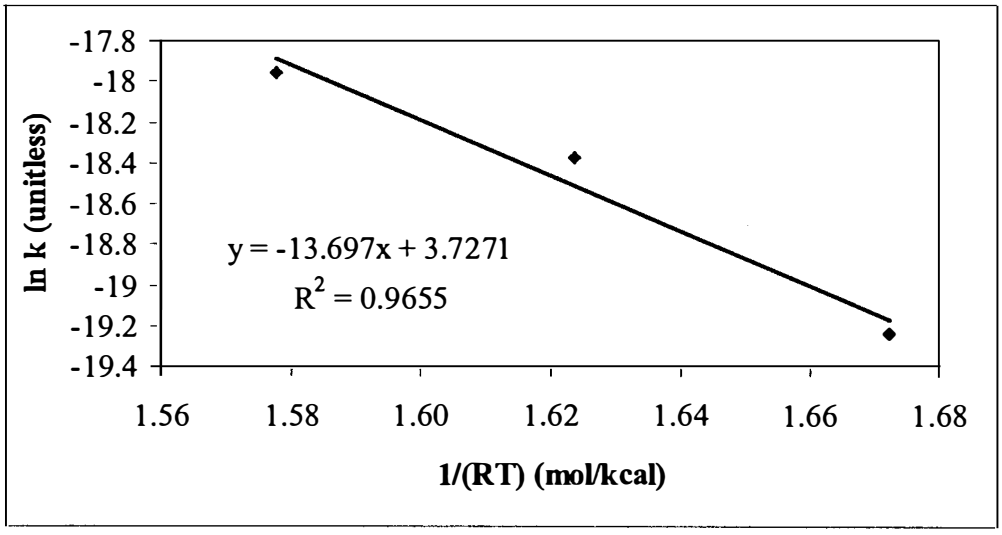

Figure 18. Determination of the activation energy and pre-exponential factor from rate constants.

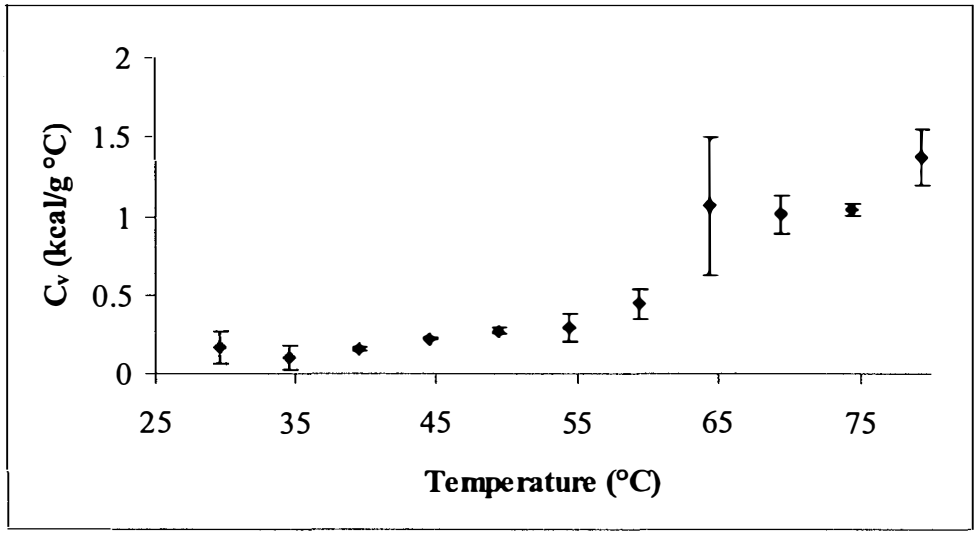

Figure 19. Heat capacity at constant volume for Aβ monomer.

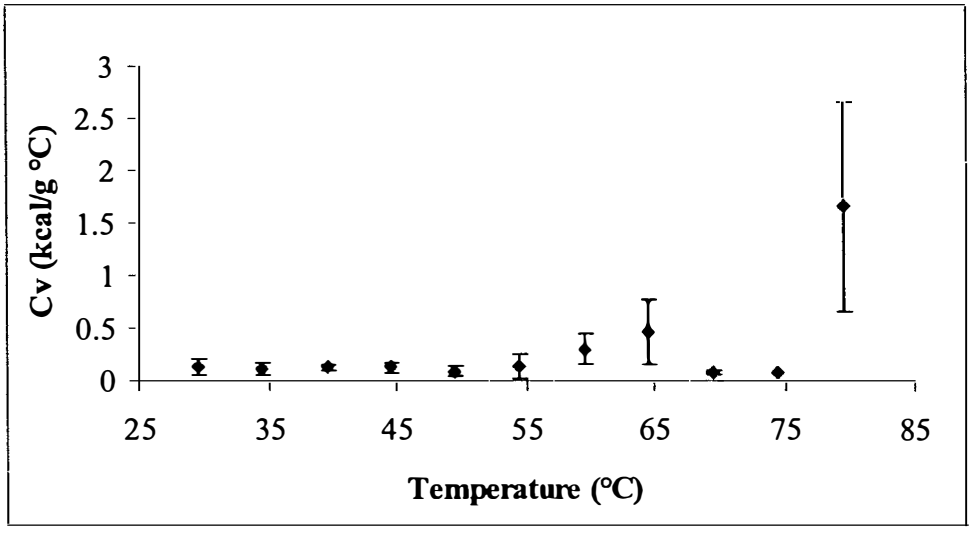

Figure 20. Heat capacity at constant volume for Aβ fibrils grown at room temperature.

by ThT assays. The critical concentration is taken when the concentration profile starts leveling off at a minimum with no significant change (<10%) between two days and when the ThT assays reaches a maximum (Figures 21 – 26 and Figure 27, respectively).

As can be seen in Figure 26, the concentration profile at 64 °C of the Aβ monomer does not follow the same trend as the rest of the concentration profiles. Once the thioflavin T fluorescence reached a maximum optical density (Figure 27) the fibrils should have stopped growing and the monomer concentration would start to level off. Instead the monomer concentration at 64 °C continues to go down at a rapid pace. The reaction at 64 °C must be at a high enough temperature that there are different processes occurring.

The critical concentration at 64 °C is taken after the first two days where the ThT assays reached a maximum. The decrease in the monomer concentration after this time may be due to conformational changes within the system or chemical reactions of the peptide. The values of the critical concentration for every temperature can be seen in Table 7 and Figure 28.

4.3.1 Van't Hoff Analysis

A van't Hoff analysis is based on thermodynamic relationship between the Gibbs Free Energy (ΔG), Enthalpy (ΔH), and Entropy (ΔS) (Equation 13) (Alberty, 1997).

$$\frac{\Delta G}{T} = \frac{\Delta H}{T} - \Delta S \tag{13}$$

ΔG can be determined by using the equilibrium constant (K_{eq}) in the following equation.

$$\Delta G = -RT\ln\left(K_{eq}\right) \tag{14}$$

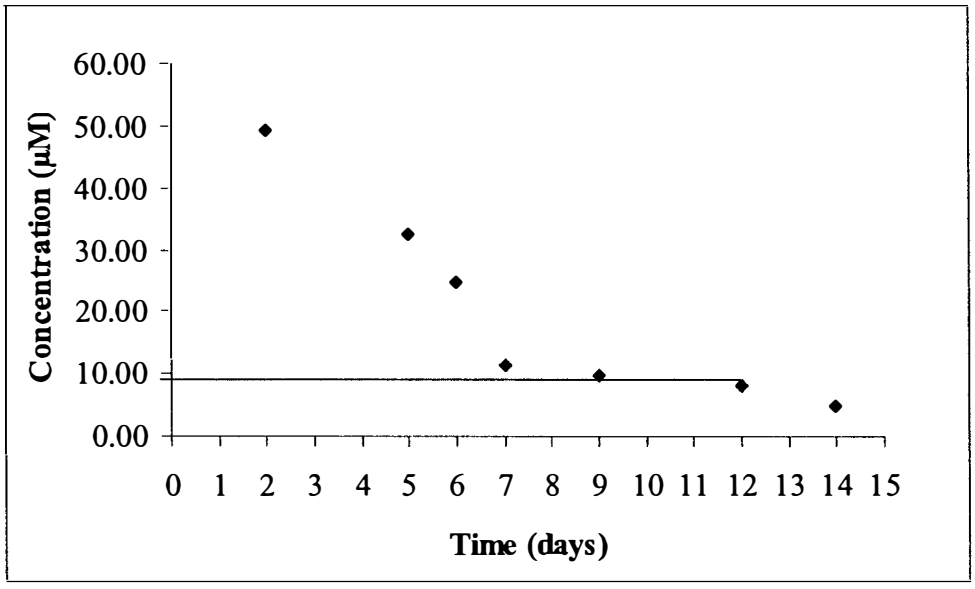

Figure 21. Concentration profile of the Aβ monomer in a 2% seeded elongation reaction at 19 °C with an initial concentration of 143.19 μM (line represents critical concentration inferred from data).

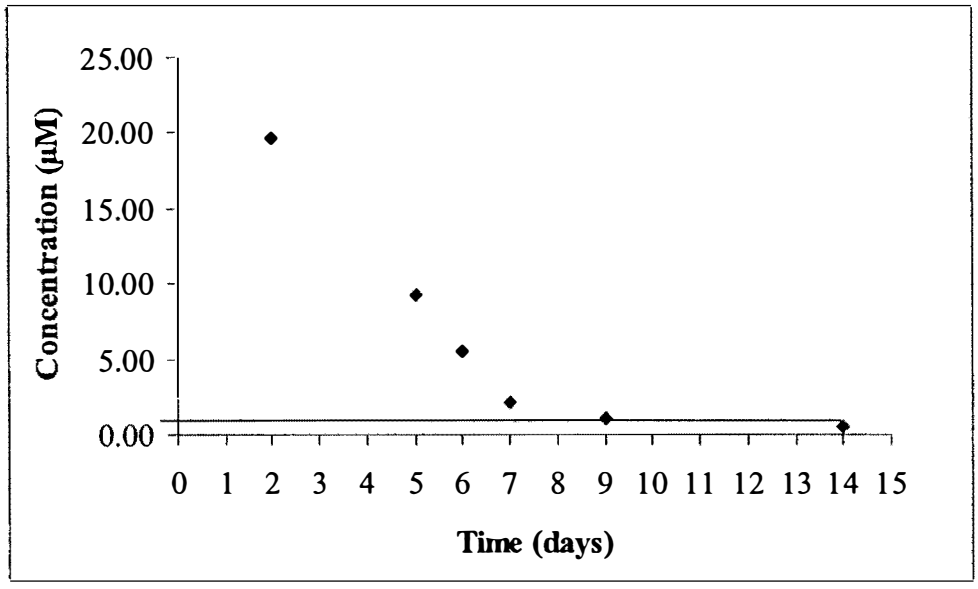

Figure 22. Concentration profile of the Aβ monomer in a 2% seeded elongation reaction at 28 °C with an initial concentration of 143.19 μM (line represents critical concentration inferred from data).

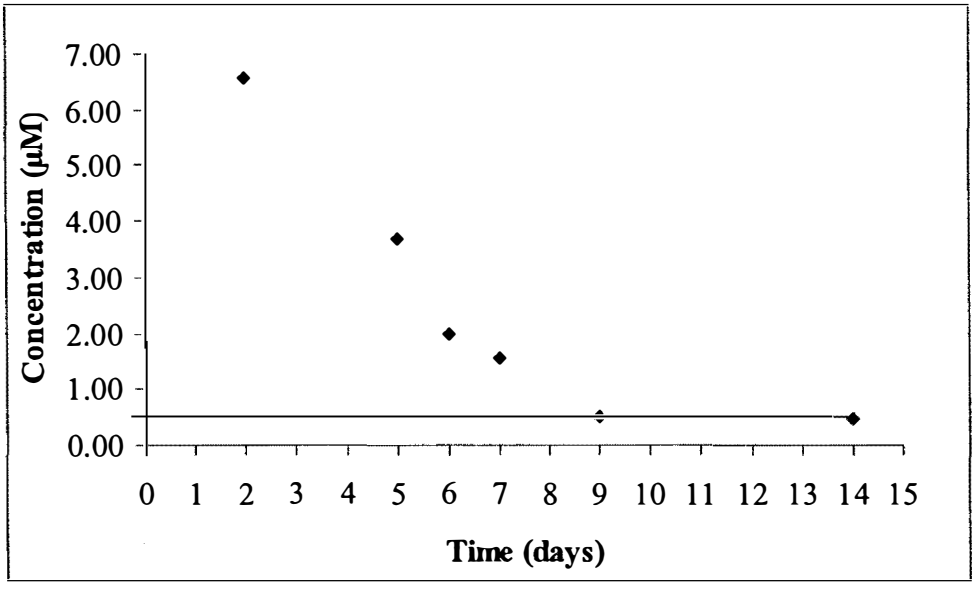

Figure 23. Concentration profile of the Aβ monomer in a 2% seeded elongation reaction at 37 °C with an initial concentration of 143.19 μM (line represents critical concentration inferred from data).

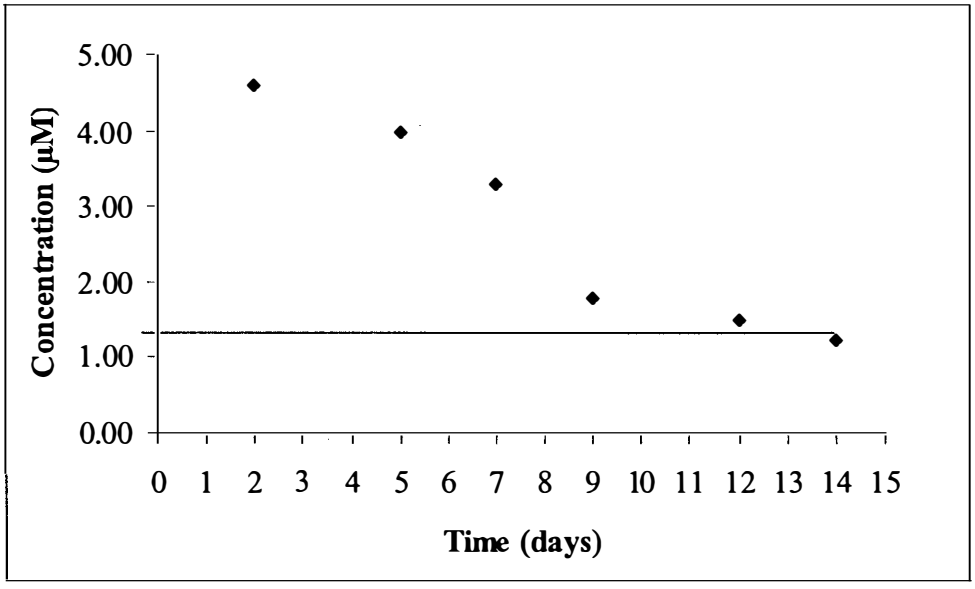

Figure 24. Concentration profile of the Aβ monomer in a 2% seeded elongation reaction at 46 °C with an initial concentration of 143.19 μM (line represents critical concentration inferred from data).

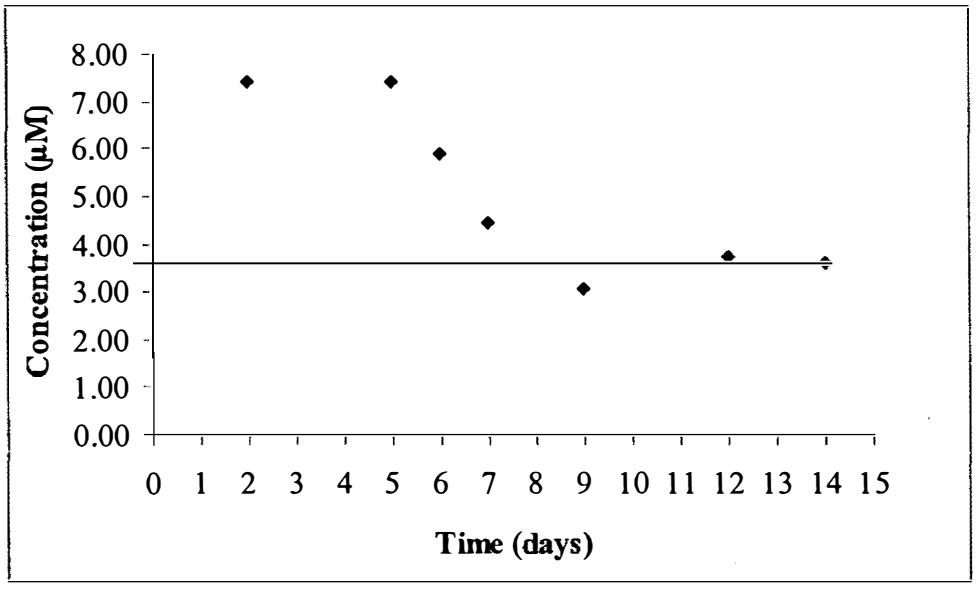

Figure 25. Concentration profile of the Aβ monomer in a 2% seeded elongation reaction at 55 °C with an initial concentration of 143.19 μM (line represents critical concentration inferred from data).

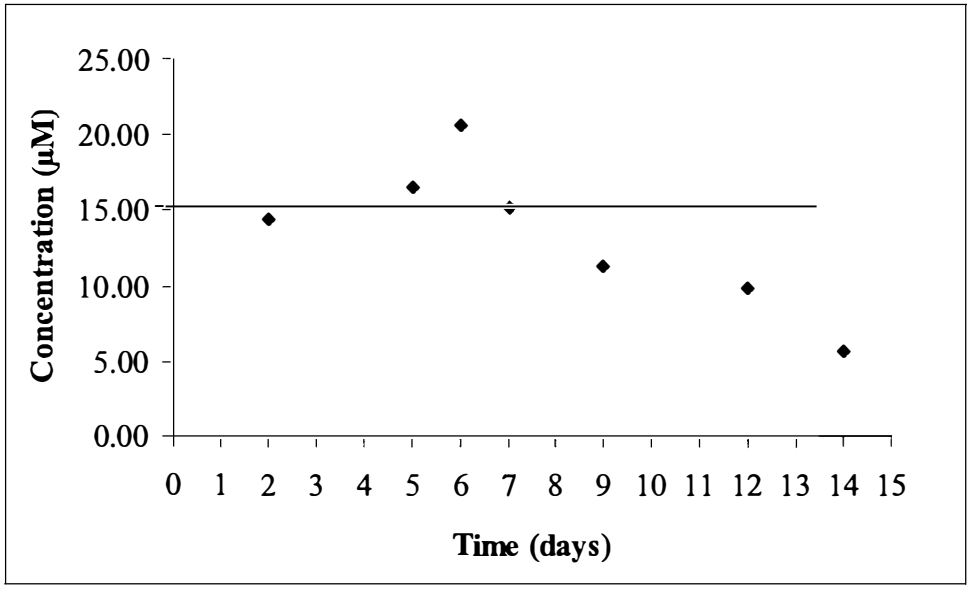

Figure 26. Concentration profile of the Aβ monomer in a 2% seeded elongation reaction at 64 ºC with an initial concentration of 143.19 μM (line represents critical concentration inferred from data).

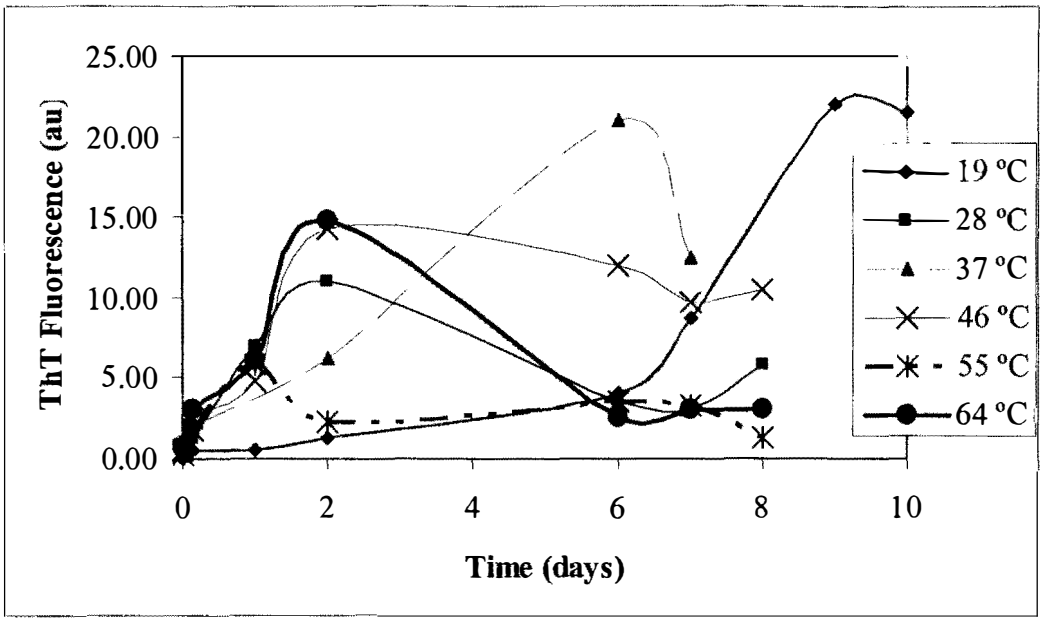

Figure 27. Thioflavin T fluorescence for a 2% seeded Aβ monomer aggregation reaction.

Table 7. Critical Concentrations of the Aβ Protein.

Temperature (°C)	Concentration (μM)
19	8.14 ± 1.65
28	1.72 ± 0.49
37	0.52 ± 0.05
46	1.62 ± 0.78
55	3.32 ± 0.66
64	15.44 ± 0.56

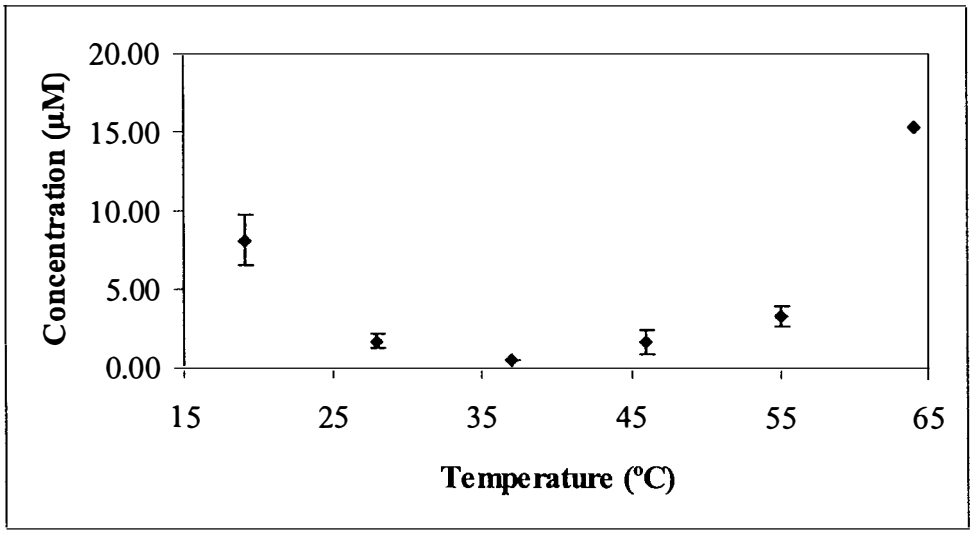

Figure 28. Critical concentration for a 2% seeded Aβ monomer aggregation reaction.

K_{eq} comes from the following reaction involving Aβ monomer attaching to fibrils, $Fibril_n + A\beta_{mon} \Leftrightarrow Fibril_{n+1}$. Since K_{eq} is defined as concentration of products divided by the concentration of reactants, the expression for Keq can be seen in Equation 15. The mass weight of the fibrils change with each addition of monomer but the molar

$$K_{eq} = \frac{[Fibril_{n+1}]}{[Fibril_n][A\beta_{mon}]} \tag{15}$$

amount of fibrils stays the same. This leads to a cancellation of the fibril concentrations in the expression for K_{eq} (Equation 16).

$$K_{eq} = \frac{1}{[A\beta_{mon}]} \tag{16}$$

By definition of K_{eq} the monomer concentration is at equilibrium, i.e. the monomer concentration is the critical concentration. The values for K_{eq} and ΔG are listed in Table 8. For a van't Hoff analysis, a plot of $\frac{\Delta G}{T}$ versus $\frac{1}{T}$ should yield a straight line with a slope of ΔH and y-intercept of ΔS (Figure 29).

For the Aβ aggregation reaction, the van't Hoff analysis in Figure 29 does not yield a straight line. It does yield two distinct straight lines with a common point at 37 °C. The different lines could represent a different set of coupled reactions in elongating the fibrils instead of the elementary equilibrium reaction that the fibril elongation was assumed to be in performing a van't Hoff analysis. Figures 30 and 31 show the van't Hoff analysis split into a high and low temperature range, respectively, with 37 °C on each of the figures. The van't Hoff predicted enthalpy of reaction (ΔH) and entropy (ΔS) from Equation 13 are listed in Table 9.

Table 8. Keq and ΔG values.

T (°C)	K_{eq} x 10^{-5} (M^{-1})	ΔG (kcal/mol)
19	1.24 ± 0.25	-6.80 ± 0.12
28	6.43 ± 2.95	-7.97 ± 0.26
37	19.12 ± 1.73	-8.91 ± 0.06
46	6.59 ± 3.18	-8.47 ± 0.31
55	3.04 ± 0.60	-8.22 ± 0.13
64	0.648 ± 0.002	-7.42 ± 0.02

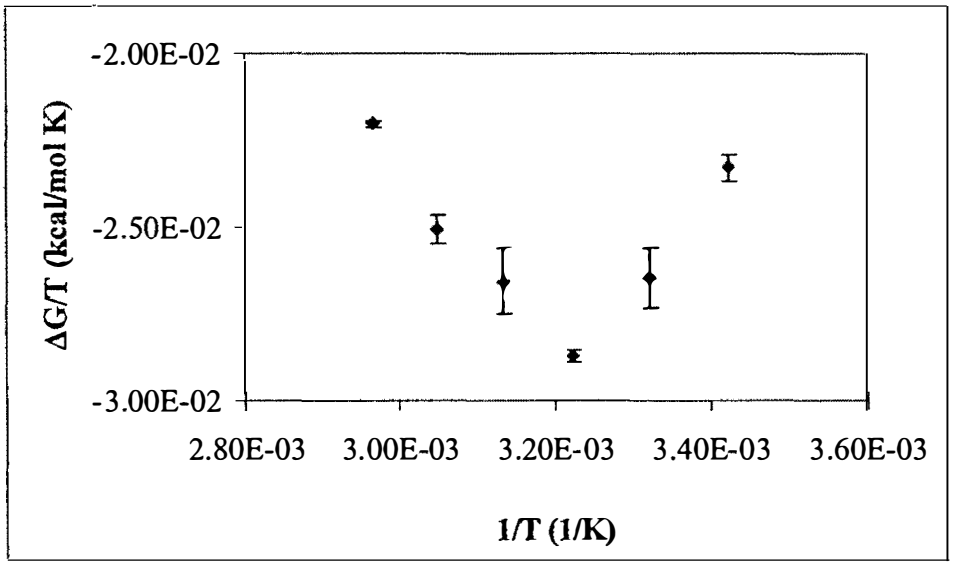

Figure 29. Van't Hoff analysis of the Aβ fibril elongation reaction.

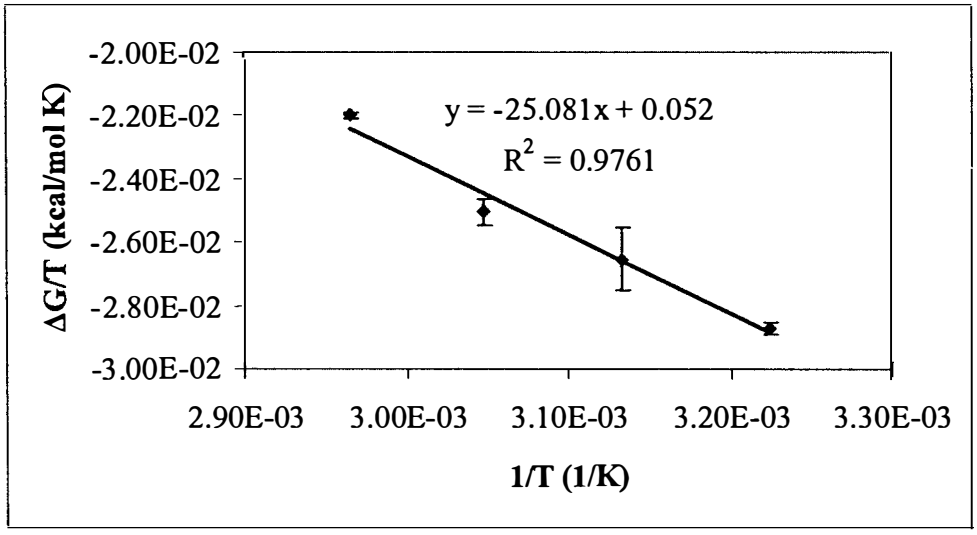

Figure 30. Van't Hoff analysis of Aβ fibril elongation reaction from 37 °C to 64 °C.

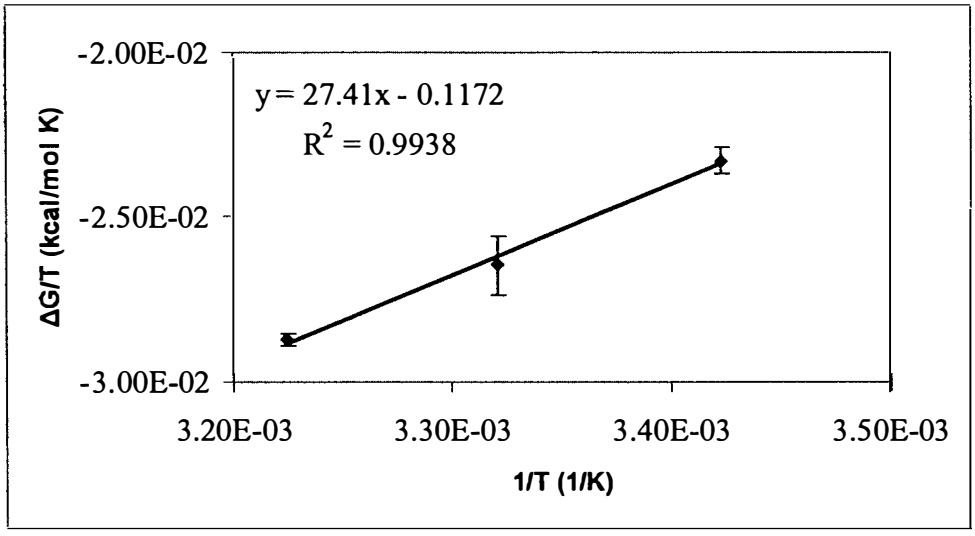

Figure 31. Van't Hoff analysis of Aβ fibril elongation reaction from 19 °C to 37 °C.

Table 9. Van't Hoff predicted enthalpy and entropy.

	ΔH (kcal/mol)	**ΔS (cal/mol K)**
Low Temperature	27.41 ± 0.18	117.20 ± 0.57
High Temperature	-20.73 ± 0.18	-38.20 ± 0.57

4.4 Comparison of van't Hoff and DSC Determined Enthalpy

Table 10 lists the ratio of the DSC determined enthalpy of fibril elongation to the van't Hoff predicted enthalpy. The enthalpy from the DSC indicates that the reaction is endothermic above 37 °C whereas the van't Hoff analysis predicts the reaction is exothermic, so the ratio at 46 °C is not listed.

Table 10. Ratio of the enthalpy of elongation from the DSC to the van't Hoff predicted enthalpy.

Temperature (°C)	**DSC Enthalpy ($kcal/mol_P$)**	**van't Hoff Enthalpy ($kcal/mol_P$)**	**Ratio of Enthalpies**
28	48,000	27	1,738
37	110,000	27	4,028
46	91,000	-25	N/A

Chapter 5. Discussion

5.1 Heat of Reaction

The heat of reaction serves an important role in understanding the overall process of fibril elongation. The heat of reaction leads to determining the reaction order, reaction rate constant, and activation energy. These are fundamental properties of the fibril elongation reaction that are not consistently documented in literature while the enthalpy is completely un-documented in the literature to date.

The equilibrium constant is at a maximum at 37 °C. This implies, as described previously, that the concentration of monomer is lowest at 37 °C and larger at 28 °C and 46 °C. The maximum in the equilibrium constant means that more monomer has reacted to elongate the fibrils at 37 °C than at the other temperatures studied. Since more monomer molecules reacted with the fibrils at 37 °C, the enthalpy change will be a maximum compared to the enthalpy changes at 28 °C and 46 °C.

5.1.1 Reaction Order, Rate, and Activation Energy

The conclusion from our analysis, that the reaction order for Aβ fibril elongation is third order overall is at odds with published literature values determined by directly following the Aβ monomer concentration. Naiki et al. (1999) found that the fibril elongation reaction is described by a pseudo first order kinetic expression written in terms of monomer concentration. The discrepancies in reaction order may arise from the large enthalpy change associated with the buffer as described previously. Naiki et al.

(1999) followed monomer concentration directly to determine reaction order whereas this study used the integral of the power output curve as described previously. A reaction order of three indicates that three entities come together simultaneously to form the product. In the case of fibril elongation, these three entities may be (a) three monomer molecules, (b) one monomer molecule, one fibril molecule, and an entity in the buffer, or (c) any three entities in the solution. At this point the three entities are not known. However, a technique (such as DSC) that measures the reaction enthalpy change may yield an overall reaction order different than a technique in which the concentration of a single species followed.

The rate constants were calculated from the regression lines associated with the reaction order data (Figures 15, 16, and 17). The rate constants show that the rate of fibril elongation increases with temperature as expected. This increase is expected due to the rate constant's dependence on temperature as described previously. The rate constants determined in this analysis can not be directly compared to works such as Cannon et al. (2004) who used surface plasmon resonance biosensors to evaluate the kinetics of Aβ fibril elongation. The rate constant in this analysis are for a third order reaction whereas in Cannon et al. the rate constants are for a first order reaction.

The activation energy from this analysis is determined with the relationship to the rate constants as described previously. The free energy of the reaction must overcome the activation energy if product is to be produced. The activation energy determined from this research, 13.7 kcal/mol, is consistent with that of Hasegawa, et al. (2002) with a published value of 10 kcal/mol. The published value of Hasegawa et al. was determined with a different buffer; their buffer was 50 mM phosphate buffer and 100 mM NaCl.

Also, their value was determined using surface plasmon resonance based on pseudo first order kinetics whereas in this research it is based on a reaction in a stationary liquid phase shown to be third order overall. The surface plasmon resonance is a technique where the fibrils are attached to a metal surface as the monomer is passed by at a predetermined velocity in a buffer solution (Hasegawa, 2002).

5.2 Heat Capacity

The heat capacity is the measurement of the internal molecular motion in a system. Internal molecular motion is central to protein folding, to protein stability, and to the protein function (Lee, 2001). The heat capacity is also associated with the packing density, which is how tightly the secondary and tertiary structures are bonded together in proteins.

When the heat capacity of a protein is linear over a temperature range, this indicates the protein is stable (that is, the molecular structure is sound and there is little molecular motion). The heat capacity data (Figures 19 and 20) shows that the Aβ monomer and fibrils are stable around 37 °C. In fact, the fibrils are stable over a temperature range of 27 °C to 60 °C. From the evident stability, we can infer that the bonds between atoms and β-sheets are not breaking apart. As the heat capacity becomes nonlinear, this indicates that the overall stability of proteins decreases (Figures 32 and 33) (Creighton, 1992).

Proteins that destabilize as temperature increases exhibit a significant increase in the heat capacity of the protein relative to the more stable state (Creighton, 1992 and Ott,

2000). The significant increase in the heat capacity is where the protein's molecules are rapidly moving and the initial secondary and tertiary structure is starting to be lost; this is called heat denaturation. Denaturation is a process where a protein in a native state (the state populated under native conditions, normally a well folded globular structure) under the influence of heat or other stressful conditions causes the protein to unfold.

When the slope of the heat capacity as function of temperature is large compared to the slope around the native state, this indicates that significant fluctuations of the protein's structure are occurring until the temperature of heat denaturation is reached, where it unfolds in a cooperative (thermodynamically favorable) manner (Dragan, 2004). The slope at 37 °C, the native state, for the fibrils is 0.02 ± 0.005 kcal g^{-1} K^{-1} whereas compared to the slope at 80 °C is 0.5 ± 0.4 kcal g^{-1} K^{-1}. Even though the 95% confidence intervals tend to be large at the higher temperatures, the data shows at least a five fold increase in slope from the native to denatured states. The heat capacity of the fibrils is still increasing so the temperature of denaturation has not been reached. After denaturation, the slope of the heat capacity will be small due to a stable conformation at higher temperatures has been reached (Dragan, 2004).

The monomer is thought to be a random coil (Selkoe, 1991). It is a commonly held belief that random coils will not denature; however the higher heat capacity values at higher temperatures show that the molecules are moving rapidly within the Aβ monomer as compared to lower temperatures. In Figure 33, the data suggests that the monomer is rearranging into a different conformation with a higher heat capacity at temperatures of 65 °C and above. A ΔC_v value that is large compared to the heat capacity of the native state of a protein indicates that the protein has changed conformation (Dragan, 2004).

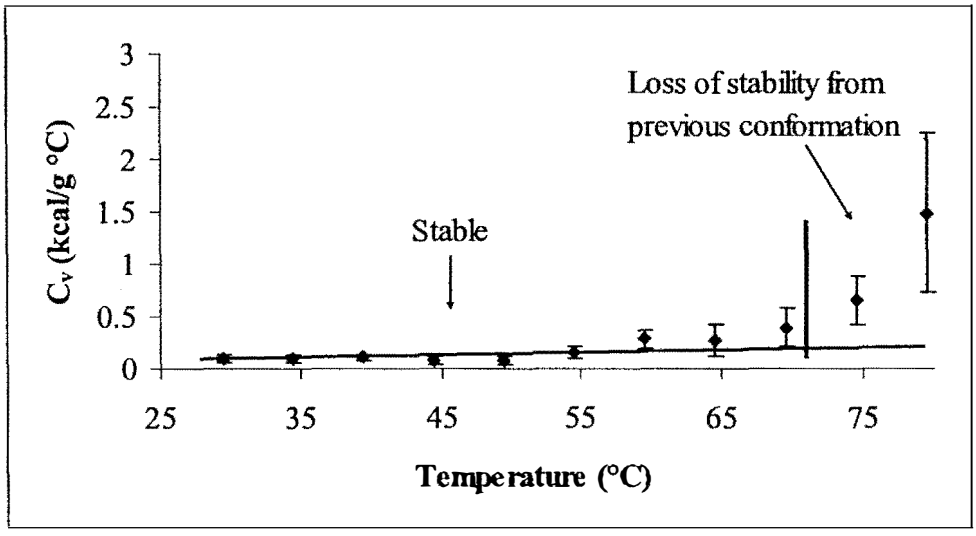

Figure 32. Heat capacity of fibrils.

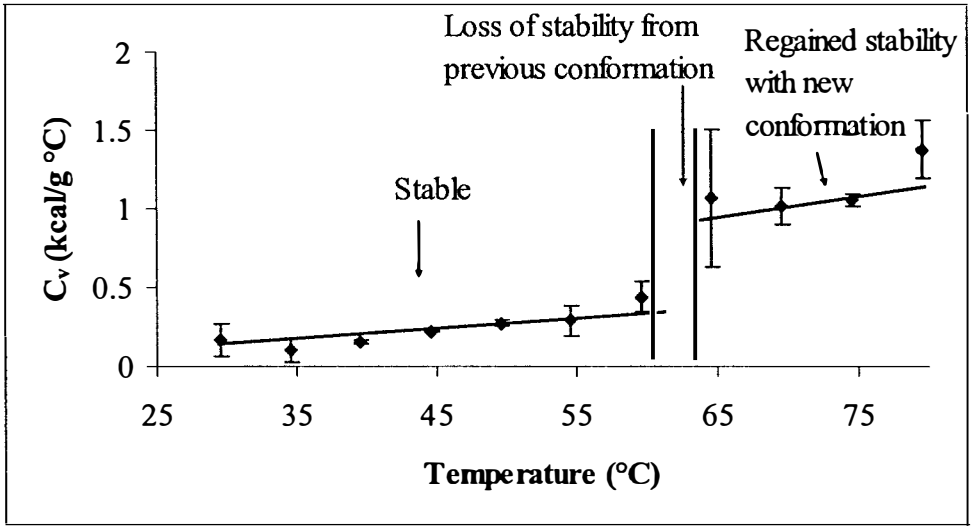

Figure 33. Heat capacity of the Aβ monomer.

For this analysis, the ΔC_v (0.5 ± 0.1 kcal g^{-1} K^{-1}) between the native state of the monomer (taken at 37 °C) and the monomer at any point above 65 °C is large relative to the heat capacity at 37 °C (0.08 ± 0.01 kcal g^{-1} K^{-1}). This appears to show that the monomer has changed from the random coil that it was in at 37 °C to a new conformation. The smaller the slope of the line through the heat capacity values, the higher the rigidity of the initial structure of the monomer. In this case, an increase in temperature does not significantly intensify fluctuations of its structure (Dragan, 2004). The conformation of the monomer above 65 °C appears to be stable in this analysis.

5.3 Critical Concentration

The critical concentration of 0.548 μM at 37 °C reported in this work is bracketed by other values reported in literature; Hasegawa et al. (2002) reported a critical concentration of 0.2 μM and Williams et al. (2004) reported 0.9 ± 0.2 μM. The critical concentrations reported in this research are taken when there is no significant change in monomer concentration from day to day except for 64 °C where the critical concentration was taken when the ThT reached a maximum. Williams et al. (2004) reports the critical concentration as the point where the monomer concentration profile starts to level off at a minimum. This is one potential source of the minor differences between the critical concentration between this research and that of Williams et al. Hasegawa et al. used a different buffer and the surface plasmon resonance used is based on a flow of monomer over the fibrils. The measured value from Hasegawa et al. (2002) came from experiments with decreasing concentrations of monomer in the flow over the fibrils that

did not produce optical changes instead of a solution of Aβ monomer in equilibrium with the fibrils. As can be seen in Figures 21 – 26, the point at which equilibrium is reached is subject to some interpretation. It would not be surprising to be some differences in reported values for the critical concentration when different methods and different criteria are used for determining when equilibrium between the Aβ monomer and fibrils are reached.

The minimum seen in the critical concentration of the monomer at 37 °C is seen in the equilibrium constant and the Gibbs free energy. The possible reasons for the minimum will be discussed in terms of the Gibbs free energy.

From the critical concentration, with some assumptions previously described, the equilibrium constant is calculated. The equilibrium constant determined in this research at 37 °C is $1.9 \times 10^{6}\ M^{-1}$ whereas Hasegawa et al. (2002) reports a value of $5 \times 10^{7}\ M^{-1}$. The difference in these reported values comes from the difference in critical concentration as described previously.

The Gibbs free energy is calculated from the equilibrium constant as described previously. The Gibbs free energy is this analysis is calculated to be -9 kcal/mol. Hasegawa et al. report -11 kcal/mol. This is reasonably good agreement between values that were determined by different techniques, as described earlier.

The Gibbs free energy profile shows a minimum at 37 °C (Figure 29). If the fibril elongation reaction is assumed to be reversible, Le Chatelier's Principle implies that the forward reaction of fibril elongation would have to be exothermic to allow for the equilibrium to shift back toward the reactants thus leading to an increase in Aβ monomer concentration at higher temperatures. Conversely, the reversible reaction would need to

be endothermic to produce an increase in monomer concentration at lower temperatures. A set of reactions with enthalpies as just mentioned will allow for the monomer concentration to increase with increasing and decreasing temperature. The equilibrium constant which is directly related to the critical concentration by Equation 16 will have a maximum at 37 °C. The equilibrium constant has an inverse relationship with the Gibbs free energy as seen in Equation 14, thus leading to the observed minimum in the Gibbs free energy at 37 °C.

The observation of a minimum in the critical concentration at 37 °C can be explained by supposing the Aβ fibril is at its most stable conformation at this temperature and becomes more unstable the further the temperature deviates from 37 °C. A protein that exhibits cold denaturation will be destabilized at low temperatures whereas one that exhibits heat denaturation will be destabilized at higher temperatures (Creighton, 1992). The less stable the fibril, the less likely that the fibril can fold to form binding sites for the monomer to attach thus increasing the critical concentration and Gibbs free energy above and below 37 °C.

5.3.1 Van't Hoff Analysis

Using the Gibbs free energy profile over the studied temperatures, the enthalpy of reaction and the entropy is determined from a van't Hoff analysis. The observation that the enthalpies of reaction above and below 37 °C determined by the van't Hoff analysis are of the same magnitude implies that there is an inverse relationship between the processes involved in the low and high temperature ranges. The inverse relationship between the enthalpy changes from the van't Hoff analysis may be the result of the

protein exhibiting cold and heat denaturation as discussed above. In cold denaturation there is a negative heat effect (endothermic) whereas in heat denaturation, there is a positive heat effect (exothermic) (Griko, 1992). The existence of a biphasic response to temperature centered around 37 °C would explain why the van't Hoff analysis appears to predict the enthalpy associated with cold and heat denaturation which is the enthalpy change associated with the folding of the monomer and fibrils into a different conformation as compared to the native state. This also implies that the folding of the monomer and fibrils are much more significant than the enthalpy associated with the attachment of monomer to the fibrils.

Equation 13 shows that the Gibbs free energy associated with a process (such as fibril elongation) has an enthalpic and entropic component. When one component is much larger than the other, it is said to control the process. The enthalpy values given in Table 8 imply that the fibril elongation reaction below 37 °C is being controlled by the large positive value of the entropy. At temperatures above 37 °C the entropy is small compared to the enthalpy below 37 °C (-52 to 117, respectively) and negative, with the result that the $-T\Delta S$ term is positive. Therefore the effect of entropy above 37 °C is to decrease the spontaneity of the reaction (that is to decrease the rate at which the reaction occurs). The negative enthalpy (indicating an exothermic reaction) is large enough in magnitude to overcome the entropic effect (as measured by the value of $-T\Delta S$ term) and drive the reaction forward above 37 °C.

5.4 Comparison of van't Hoff and DSC Determined Enthalpy

The fibril elongation consists of the Aβ monomer and fibril ends folding to form binding sites and the attachment of the monomer to the fibrils at these sites (Lomakin, 1997). There should be different enthalpies associated with the folding of the monomer and fibrils and with the attachment of monomer to fibrils that the DSC measures. This leads to a difference in the van't Hoff prediction of enthalpies and the DSC measured enthalpies. A van't Hoff analysis is based on an elementary reaction with reactants going to products with no intermediates, side reactions, or folding and, in solutions; reactions are generally more complex than indicated by simple chemical equations (Liu, 1997). This discrepancy in the enthalpy of fibril elongation from the DSC means that the calorimetric enthalpy change will always be higher than the enthalpy change that the van't Hoff analysis predicts. Although, for this analysis, previously discussed problems with the enthalpy change associated with the buffer could lead to a higher enthalpy from the DSC than the van't Hoff analysis predicts.

In this study, the experimentally determined enthalpy values from the DSC are compared to the predicted enthalpy values from the van't Hoff analysis. A ratio of the experimental enthalpy from the DSC to the van't Hoff enthalpy higher than one is believed to represent the presence of intermediates in the experimental reaction (Zhuang, 1994) because the enthalpy changes associated with the intermediate reactions are summed together along with the reaction of interest. The van't Hoff analysis does not take into account intermediates. Liu et al. (1997) show that for different proteins the calorimetric measured enthalpy changes are greater than the predicted enthalpy change

from the van't Hoff analysis. Liu et al. also showed that the van't Hoff enthalpy change becomes more negative with increasing temperature while the calorimetric enthalpy change becomes less negative.

Kirkitadze, et al., (2001) have identified numerous intermediates in the aggregation reaction of Aβ monomer to fibril. With the high amount of Aβ monomer in solution and the amount of time that the experiment lasts, it is reasonable to speculate that intermediate reactions are occurring at the same time as the fibril elongation reaction.

With the assumption that there are no unwanted aggregates in the Aβ monomer solution while the experiment is being performed and with the appearance that the van't Hoff predicted enthalpies are the enthalpies of cold and heat denaturation, the DSC enthalpy will be higher than the van't Hoff. The higher enthalpy values in the DSC is because denaturation does not represent a single two state transition but includes several stages due to complex profile (Creighton, 1992). But with the problems associated with the enthalpy change of the buffer it is hard to draw conclusions with confidence for this analysis.

Chapter 6. Conclusions

The object of this research was to experimentally determine thermophysical properties of the Aβ protein and the fibril elongation reaction such as enthalpy, entropy, activation energy, reaction rate constants, and heat capacities. This research has examined the use of a differential scanning calorimeter to obtain thermophysical properties from differential scanning calorimetry. Problems associated with the large enthalpy change of the buffer alone led to uncertainty in the values of the physical property measurements.

In future work, to directly determine the enthalpy of fibril elongation, a different solution should be used that will not yield as large an enthalpy change as the NaOH – 2X PBS buffer. Other solutions could include water or just the NaOH in a nitrogen environment, to eliminate the reaction of the NaOH with air. Once the details of the buffer can be worked out, the enthalpy of the Aβ fibril elongation reaction along with reaction order, rate constants, and activation energy should be accurately determined. Then it would be feasible to move on to other amyloid disease-causing proteins.

LIST OF REFERENCES

List of References

Alberty, R. A. and Silbey, R. J. *Physical Chemistry.* 2nd Edition. New York: John Wiley & Sons, Inc., 1997.

Benson, S. W. *The Foundations of Chemical Kinetics.* New York: McGraw-Hill, Inc., 1960.

Briggs, L. 1943. (4/15/2005) http://ts.nist.gov/ts/htdocs/230/232/ARCHIVED_CERTIFICATES/49b.pdf

Cannon, M. J., Williams, A. D., Wetzel, R., and Myszka, D. G. (2004). "Kinetic analysis of beta-amyloid fibril elongation." Analytical Biochemistry **328**: 67 – 75.

Creighton, T. E. (Editor). *Protein Folding.* New York: W. H. Freeman and Co., 1992.

Dragan, A. I., Potelchin, S. A., Sivolob, A., Lu, M., and Privalov, P. L. (2004). "Kinetics and Thermodynamics of the unfolding and refolding of the Three-Standard α-helical coiled coil, Lpp-56." Biochemistry **43**: 14891 – 14900.

Fezoui, Y., Hartley, D. M., Harper, J. D., Khurana, R., Walsh, D. M., Condron, M. M., Selkoe, D. J., Lansbury Jr., P. T., Fink, A. L., and Teplow, D. B. (2000). "An improved method of preparing the amyloid β-protein for fibrillogenesis and neurotoxicity experiments." Amyloid: international journal of experimental and clinical investigation: official journal of the International Society of Amyloidosis **7**: 166 – 178.

Fezoui, Y. and Teplow, D. (2002). "Kinetic Studies of Amyloid β-Protein Fibril Assembly." The Journal of Biological Chemistry **277**: 36948 – 36954.

Friedli, G. L. (1996). "Interaction of Deamidated Soluble Wheat Protein (SWP) with other Food Proteins and Metals." Doctoral Dissertation, The University of Surrey, 1996. http://www.friedli.com/research/PhD/DSC/chap3.html (1/27/2005).

Griko, Y. V. and Privalov, P. L. (1992). "Calorimetric Study of the Heat and Cold Denaturation of β-Lactoglobulin." Biochemistry **31**: 8810 – 8815.

Hasegawa, K., Yamaguchi, I., Omata, S., Gejyo, F., and Naiki, H. (1999). "Interaction between Aβ(1 – 42) and Aβ(1 – 40) in Alzheimer's β-Amyloid Fibril Formation in Vitro." Biochemistry **38**: 15514 – 15521.

Hasegawa, K., Ono, K., Yamada, M., and Naiki, H. (2002). "Kinetic Modeling and Determination of Reaction Constants of Alzheimer's β-Amyloid Fibril Extension

and Dissociation Using Surface Plasmon Resonance." Biochemistry **41**: 13489 – 13498.

Kheterpal, I., Zhou, S., Cook, K. D., and Wetzel, R. (2000). "Aβ amyloid fibrils possess a core structure highly resistant to hydrogen exchange." Proceedings of the National Academy of Sciences of the United States of America **97**: 13597 – 13601.

Kirkitadze, M. D., Condron, M. M., and Teplow, D. B. (2001). "Identification and Characterization of Key Kinetic Intermediates in Amyloid β-protein Fibrillogenesis." Journal of Molecular Biology **312**: 1103 – 1119.

Kreyszig, E. *Advanced Engineering Mathematics.* 8th Edition. New York: John Wiley & Sons, Inc., 1999.

Kusumoto, Y., Lomakin, A., Teplow, D. B., and Benedek, G. B. (1998). "Temperature dependence of amyloid β-protein fibrillization." Proceedings of the National Academy of Sciences of the United States of America **95**: 12277 – 12282.

Lee, A. L. and Wand, A. J. (2001). "Microscopic origins of entropy, heat capacity and the glass transition in proteins." Letters to Nature **411**: 501 – 504.

Lomakin, A., Teplow, D. B., Kirschner, D. A., and Benedek, G. B. (1997). "Kinetic Theory of fibrillogenesis of amyloid β-protein." Proceedings of the National Academy of Sciences of the United States of America **94**: 7942 – 7947.

Liu, Y. and Sturtevant, J. M. (1997). "Significant discrepancies between van't Hoff and calorimetric enthalpies. III" Biophysical Chemistry **64**: 121 – 126.

Lynn, D. G. and Meredith, S. C. (2000). "Review: Model Peptides and the Physicochemical Approach to β-Amyloids." Journal of Structural Biology **130**: 153 – 173.

Naiki, H. and Gejyo, F. (1999). "Kinetic analysis of amyloid fibril formation." Methods in Enzymology **309**: 305 – 318.

Ott, J. B. and Boerio-Goates J. *Chemical Thermodynamics: Advanced Applications.* San Diego: Academic Press, 2000.

Selkoe, D. J. (1991). "The Molecular Pathology of Alzheimer's Disease." Neuron **6**: 487 – 498.

Selkoe, D. J. (2000). "The Origins of Alzheimer Disease. A is for Amyloid." The Journal of the American Medical Association **283**: 1615 – 1617.

Strouse, G. F. (2001). "Standard Reference Material 1745: Indium Freezing–point Standard. Reference Material 2232: Indium DSC Melting-point Standard." NIST Special Publication (SP 260-132).

Sweir, S. and Van Mele, B. (2003). "Reaction Thermodynamics of Amine-cured Epoxy Systems: Validation of the Enthalpy and Heat Capacity of Reaction as Determined by Modulated Temperature Differential Scanning Calorimetry." Journal of Polymer Science: Polymer Physics **41**: 597 - 608.

Taylor, B. M., Sarver, R. W., Fici, G., Poorman, R. A., Lutzke, B. S., Molinari, A., Kawabe, T., Kappenman, K., Buhl, A. E., and Epps, D. E. (2003). "Spontaneous Aggregation and Cytotoxicity of the β-Amyloid $A\beta^{1-40}$: A Kinetic Model." Journal of Protein Chemistry **22** (1): 31 – 40.

Tjernberg, L. O., Tjernberg, A., Bark, N., Shi, Y., Ruzsicska, B. P., Bu, Z., Thyberg, J., Callaway, D. J. E. (2002). "Assembling Amyloid Fibrils from designed structures containing a significant amyloid β-peptide fragment." Biochemical Journal **366**: 343 – 351.

Todd, M. J. and Gomez, J. (2001). "Enzyme Kinetics Determined Using Calorimetry: A General Assay for Enzyme Activity?" Analytical Biochemistry **296**: 179 - 187.

Walsh, D. M., Lomakin, A., Benedek, G. B., Condron, M. M., and Teplow, D. B. (1997). "Amyloid β-Protein Fibrillogenesis. Detection of a Protofibrillar Intermediate." The Journal of Biological Chemistry **272** (35): 22364 – 33372.

Walsh, D. M., Hartley, D. M., Condron, M. M., Selkoe, D. J., and Teplow, D. B. (2001). "In vitro studies of amyloid β-protein fibril assembly and toxicity provide clues to the aetiology of Flemish variant ($Ala^{692} \rightarrow$ Gly) Alzheimer's disease." Biochemical Journal **355**: 869 – 877.

Williams, A. D., Portelius, E., Kheterpal, I., Guo, J., Cook, K. D., Xu Y., and Wetzel, R. (2004). "Mapping Aβ amyloid fibril secondary structure using scanning proline mutagenesis." Journal Molecular Biology **335**: 833 – 842.

Xing, Y. and Higuchi, K. (2002). "Amyloid fibril proteins." Mechanisms of Ageing and Development **123**: 1625 – 1636.

Zhuang, P., Eisenstein, E., and Howell, E. E. (1994). "Equilibrium Folding Studies of Tetrameric R67 Dihydrofolate Reductase." Biochemistry **33**: 4237 – 4244.

Žerovnik, E. (2002). "Amyloid-fibril formation. Proposed mechanisms and relevance to conformational disease." European Journal of Biochemistry **269**: 3362 – 3371.

VITA

Donald Edward Hicks was born in Bristol, Tennessee on August 28, 1978. He graduated from Sullivan East High School in Bluff City, Tennessee in June of 1996. In August, 1996 he entered The University of Tennessee, Knoxville and in May, 2001 received a degree of Bachelor of Science in Chemical Engineering. He entered The University of Tennessee, Knoxville in August, 2003 and in May, 2005 received a Master of Science in Chemical Engineering.